EVALUATION OF THE DEGRADATION OF METHYLENE BLUE USING PHOTOCATALYTIC MATERIALS

A THESIS IN
Civil Engineering

Presented to the Faculty of the University of
Missouri-Kansas City in partial fulfillment of
the requirements for the degree

MASTER OF SCIENCE

by
HANNAH M. MCINTYRE

B.S., University of Missouri-Kansas City, 2020

Kansas City, Missouri
2021

EVALUATION OF THE DEGRADATION OF METHYLENE BLUE USING PHOTOCATALYTIC MATERIALS

Hannah M. McIntyre, Candidate for the Master of Science Degree

University of Missouri-Kansas City, 2021

ABSTRACT

Non-point organic pollutants in groundwater, stormwater, wastewater, and drinking water are a growing problem in the environment, which lack effective and efficient treatment technologies. Photocatalytic treatment of organic contaminants in aqueous or liquid mediums has gained interest due to their potential for effective degradation. Common industrial treatment practices utilize a slurry reactor, suspending the photocatalyst in the contaminated solution. However, photocatalytic slurry reactors are hindered by solution turbidity, dissolved salt content, and absorbance of light. Research presented here introduces two novel engineered material combinations which immobilize the photocatalyst for effective and sustainable degradation of organic pollutants, one in-situ and one ex-situ. Methylene blue was chosen as a surrogate contaminant for both studies considering well studied degradation pathway literature.

The in-situ method investigates immobilizing titanium dioxide in cement paste by functionalizing it with maleic anhydride (Ti-MAH). This process not only immobilizes the photocatalyst but also increases the reactivity of the catalysts. Preparation of the Ti-MAH is performed by permanently bonding the maleic anhydride to titanium dioxide in methanol, drying and powdering residual material, and then inter-grinding the preparation with cement during mixing. When compared with OPC, the Ti-MAH cured cement paste is more

reactive under a wider range of light wavelengths, possesses a higher band gap, sustains this heightened reactivity over multiple testing iterations, and treats organics effectively. Amorphous silica within the calcium-silica-hydrate, C-S-H, is theorized to bond to the powdered Ti-MAH during curing. Verification of silica bonding to the titanium by way of MAH was demonstrated by FTIR spectra, SEM imagery, and XRD. Creating a sustainable and passive photocatalytic cement that precisely bonds silicon to the Ti-MAH is useful for organic contaminant in urban stormwater but use can translate to other applications because the Ti-MAH bonds readily with any amorphous silica such as glass materials, paints and coatings, optics and LEDS, among many others.

The ex-situ method introduces the development and application of a novel, photocatalytic, porous silica-based granular media (SGM) to be used in a packed bed column reactor. SGM retains the cross-linked structure developed during synthesis through a combination of foaming agent addition and activation temperature. The resultant media has a high porosity of 88%, with a specific surface area averaging 150 m^2/g. Photocatalytic capabilities are further enhanced as the resultant structure fixes the photocatalyst within the translucent matrix. SGM is capable of photocatalysis combined with diffusion of nucleophiles, electrophiles, and salts from the pore space. The photocatalytic efficiencies of SGM at various silica contents were quantified in batch reactors using methylene blue destruction over time and cycles. Methylene blue concentrations of 10mg/L were effectively degraded (>90%) within 40 minutes. This effectiveness was retained over multiple cycles and various methylene blue concentrations. SGM is a passive and cost-effective granular treatment system technology which can translate to other organic contaminants and industrial processes.

The two treatment methods use varying processes and materials to meet the fundamental goal of immobilizing the photocatalysts for a sustained attack on organic pollutants. The studies present the experimental methods of both remedial technologies in sequence from material development and immobilization of the photocatalysts to assessment of reactivity and longevity. Herein, batch reactors are utilized to individually test each photocatalytic material and determine their feasibility to be up-scaled into an onsite pilot-test.

APPROVAL PAGE

The faculty listed below, appointed by the Dean of the School of Computing and Engineering have examined a thesis titled "Evaluation of the Degradation of Methylene Blue Using Photocatalytic Materials," presented by Hannah M. McIntyre, candidate for the Master of Science degree, and certify that in their opinion it is worth of acceptance.

Supervisory Committee

Megan Hart, Ph.D., Committee Chair
Department of Civil Engineering

Kathleen Kilway, Ph.D.
Department of Chemistry

Jejung Lee, Ph.D.
Department of Geosciences

CONTENTS

LIST OF ILLUSTRATIONS

LIST OF TABLES

Table Page

ACKNOWLEDGEMENTS

First and foremost, I would like to thank my advisor, Dr. Megan Hart, for her consistent guidance, support, and mentorship throughout the journey of this thesis. I would also like to thank my thesis committee members, Dr. Kathleen Kilway and Dr. Jejung Lee for taking time to be apart of this journey. Finally, I would like to thank my parents and sisters for their support. Without them none of this would have been possible.

CHAPTER 1

INTRODUCTION

Light has been shown to naturally degrade and decompose organic compounds overtime through photolysis. The ability to use semiconductors to catalyze this reaction was discovered in the late 1900s. Since this discovery, photocatalysts have been utilized to degrade harmful organic pollutants in wastewaters. Current techniques at wastewater treatment plants introduce photocatalysts, most commonly titanium dioxide, in slurry reactors to the degrade organic contaminants conventional methods cannot. This procedure allows the photocatalyst to disperse within the contaminant solution and optimize surface area reactivity with UV light. One of the major drawbacks of this methods is the need to filter out the photocatalyst after treatment. There is an established need to develop destructive technologies with the capability to continuously and effectively degrade organic pollutants. Limited efforts have been made to immobilize photocatalysts considering the few investigations which have occurred have led to decreased reactivity of the catalyst. The current studies have been designed to investigate the ability to immobilize titanium dioxide into material matrixes for an improved and sustained attack on organic pollutants. Two specific studies were carried out, one for in-situ use and the other for ex-situ. The results of batch reactor experimentation on both studies is presented herein and discussed in the following manner:

- Chapter 2: Building upon the current state of knowledge of photocatalytic cement, a novel method of immobilizing titanium dioxide in the C-S-H phase of cement was developed. While titanium dioxide and maleic anhydride bonds (Ti-MAH) are well studied in literature, no known studies have introduced Ti-MAH into cement. A modified method of functionalization was validated, along with the determination of

Ti to MAH ratio. To establish an optimized Ti to MAH ratio and validate the increased reactivity, mixture proportions with variable amounts of titanium dioxide and a consistent w/c were tested. Batch reactor experiments were set up to analyze methylene blue degradation over time and cycles.

- Chapter 3: A porous, photocatalytic silica-based granular media (SGM) was developed for ex-situ remediation of organic contaminants in wet mediums. While the media was developed specifically for emerging contaminants of concern, the validation of its photocatalytic capabilities were performed using a cation dye, methylene blue, in this study. From media synthesis to batch reactor experimentation, the utilization of SGM for the degradation of organic pollutants was determined to be effective and sustainable.
- Chapter 4: Overarching conclusions between the two experimental designs are discussed, along with future testing and recommendations for implementation.

CHAPTER 2

IMMOBILIZATION OF TIO_2 NANOPARTICLES IN CEMENT FOR IMPROVED PHOTOCATALYTIC REACTIVITY AND TREATMENT OF ORGANIC POLLUTANTS

Introduction

As urban watersheds grow, the transport of organic contaminants, such as polychlorinated biphenyls (PCBs), polycyclic aromatic hydrocarbons (PAHs), organochlorine pesticides (OCPs), and per- and polyfluoroalkyl substances (PFAS), in stormwater and surface runoff has increased in occurrence and amount [1-4]. Organic contaminants are listed as priority or emerging contaminants of concern in stormwater due to their persistence in the environment and the lack of effective conventional treatment technologies. Best management practices (BMPs) within the framework of green infrastructure (GI) act to curtail and control the volume of urban runoff, but most are ineffective in organic contaminant reduction. One of the primary mechanisms for reducing urban runoff volumes as well as contaminant treatment within low impact development (LID) is permeable pavements or permeable concrete structures [5]. While various research has been done to compare permeable interlocking concrete pavers, pervious concrete, and porous asphalt [6,7], pervious concrete is preferred for contaminant reduction potential [8]. The premise of pervious concrete is to allow for stormwater quantity and intensity reduction through the flow of water into hydraulically conductive sublayers that allow for natural percolation, infiltration, and stormwater peak intensity dissipation. Permeable pavement installations have increased in usage as the practice becomes mainstream, however, adaptations are limited to relatively low traffic areas and little design consideration is given to stormwater contaminant reduction [9].

Organic Contaminants in Stormwater

While GI and LID are beginning to focus on integrating both facets of stormwater, implementation within the urban environment can be difficult [10]. Regardless of efforts to reduce stormwater production and runoff volumes, many pollutants reside in urban stormwater. Organics are one of the most concerning pollutants in urban stormwater runoff [11]. Many organics contaminants, such as hydrocarbons, pose potential harm to human health and the environment despite implementation of mainstream stormwater management practices [12]. Total petroleum hydrocarbons (TPH) are hazardous to human health and some are potentially toxic to humans [13]. Some TPH compounds such as benzene, are carcinogenic while others, such as gasoline, are listed by the International Agency for Research on Cancer (IARC) as known carcinogens when occupationally encountered during routine use [13]. Hydrocarbons from petroleum are one of the largest contributors to urban stormwater pollutant load and are generally more concentrated in heavily trafficked areas [14]. In agricultural areas increased concentrations of organic pesticides, such as organochlorine a pyrethroid, have been found in stormwater runoff [15]. Pharmaceuticals and personal care products are pollutants that have begun to emerge in urban stormwaters [16]. PFAS are more recent emerging contaminants of concern, considering they are very persistent bioaccumulative compounds, and therefore stormwater monitoring and treatment of them has become a top priority to various agencies [3,17]. PFAS elude most conventional treatment methods such as advanced oxidation processes (AOP) or membrane treatment techniques, much in part to the versatility in use, production, and high solubility in water [18]. Human health impacts of perfluorooctanoic acid (PFOA) and perfluorooctanesulfonic acid (PFOS) include liver, immunological, developmental, endocrine, reproductive, and cardiovascular, along with potential for cancer

[3]. Since the industrial switch from natural dyes to synthetic, over 100,000 synthetic dyes have been produced and have been widely associated with water pollution due to the 10-15% waste during production [19,20]. Synthetic dyes can cause numerous health effects such as respiratory sensitization, skin irritation, and asthma [19]. Considering the vast impact organic contaminants have, a method is needed to mitigate the contaminants in remaining urban stormwater [11].

Challenges and Motivation

The majority of stormwater runoff in urban areas is collected through combined or separate sewer systems and either treated at wastewater facilities or discharged via storm sewers to streams. However, the increase in runoff quantity causes infiltration and inflow into collection systems, causing wastewater treatment plants to routinely exceed storage and treatment capacities [12]. While there are many factors that impact inflow and infiltration and runoff treatment planning and management, a need for stormwater management beyond the existing GI is evident. Photocatalysis is a known degradation method in wastewater treatment that has potential for translation and integration in both impermeable and permeable concrete pavements and structures through the incorporation of a catalyst metal within the cementitious materials [21]. Degradation of contaminants during transport across or through concrete may initiate organic destruction during the time of travel, which may allow for less treatment time in receiving facilities, ultimately decreasing capacity needs. Research has shown that incorporating photocatalysts within concrete or as a surface sealant on structures results in some or partial degradation of air pollution within the immediate proximity of the surface. However, treatment capacity is not sustainability as degradation potential reduces over time

[22]. Furthermore, to date, no studies have been published on the photocatalytic ability of concrete to directly treat stormwater.

Research presented here investigates the ability of functionalized titanium dioxide (TiO_2) nanoparticles to permanently bond to silicates within cement for the purpose of photocatalytic degradation of organic contaminants in stormwater. Herein, TiO_2 was functionalized to maleic anhydride (MAH), subsequently referred to as Ti-MAH, deposited into powder form, and then introduced to ordinary portland cement (OPC) during mixing procedures. Degree of fixation and reactivity were investigated by measuring the degradation of methylene blue, a known organic contaminant surrogate test pollutant [23]. In order to assess sustainable reactivity, methylene blue dye degradation was analyzed over multiple, sequential cycles. The cement mixtures with Ti-MAH were tested against those containing only TiO_2 as well as a control mixture OPC lacking TiO_2, in order to determine the sustainability of the photocatalytic capabilities within the environment.

Photocatalytic Capabilities of TiO_2

Photocatalysts are materials capable of producing photoexcited electrons by absorbing light. Photoexcited electrons then elevate from the valence band gap to the conduction band gap and generate electron-hole pairs (e-/h+) that produce transformation of reaction participants. The resulting pair (e-/h+) act to reduce and/or oxidize compounds adjacent to the reactant surfaces making this method of contaminant treatment particularly effective for organic contaminants [24]. TiO_2, ZnO, SnO_2, and CeO_2 are heterogeneous photocatalysts that are abundant in nature and utilized in semi-conductor applications [25]. Heterogenous metal oxides such as titanium are widely used in photocatalytic applications because of the ability to produce positive electron holes that act to oxidize organic solutions and decompose water in

the presence of UV light under ambient conditions [26,27]. TiO_2 is considered a superior photocatalyst for organic pollutants in comparison to other metal oxides because it possesses photostability and low toxicity [28-30]. Band gap is a measure of energy needed to promote an electron from the valence band to the conduction band and is generally considered a measure of reactivity of the photocatalyst, eg the higher the band gap the more energy garnered during photoexcitation. Anatase has a larger band gap (3.2 eV) than rutile (3.0 eV), which has been shown to reduce the light absorbed, but increased the oxidation ability of electrons [31]. One means of increasing the band gap, increase reactivity and absorbance is to functionalize the catalyst with MAH. The addition of MAH to the TiO_2 surface has been shown to increase the band gap, thus making the photocatalyst more reactive [32].

Photocatalytic Treatment of Organic Contaminants

Photocatalytic decomposition of organic pollutants is a promising technology in which a catalyst generates a ·OH radical by oxidation of OH- anions or generation of O_2^- radicals by reduction of O_2 [33]. Organic contaminants derived from non-point sources resist treatment within traditional best management practice. In order to reduce organic contaminants from non-point sources, water is collected and treated at wastewater facilities using photocatalysis [4]. Current treatment techniques for organic contaminants in wastewater involve slurrying TiO_2 in order to optimize the surface area of reactive sites available during treatment [34]. While effective, TiO_2 slurries require secondary or membrane filtration to ensure nano particulates are not introduced to the environment as new contaminants and to quench free radical presence [35]. As our understanding of nanoparticles in the environment grows, immobilization of TiO_2 on substrates for treatment of contaminants has become more prevalent. Different methods of immobilizing TiO_2 nanoparticles have been utilized such as

bonding to activated carbon [36], plastics [37] and clays [38]. More recently, photocatalytic decomposition methods have been studied for stormwater and groundwater treatment [39,40]. The development of innovative technologies, which utilize immobilized photocatalysts, can be used to mitigate the volume of organic contaminants treated at wastewater facilities.

Photocatalytic Concrete

The capabilities of photocatalytic concrete to reduce air and organic pollutants have been extensively studied with commercially available cements. TX Active® is a commercially available cement containing TiO_2 and has been industrialized in Italy, France, and Belgium [41], along with the United States [42]. The inclusion of TiO_2 in pervious concrete has been shown to degrade air pollutants as well [8]. However, the efficiency of a photocatalyst mixed within the concrete structure has been questioned due to the limited amount of photocatalyst exposed to the surface [43]. Therefore, various forms of photocatalytic coatings have been produced to optimize the surface area of the photocatalyst exposed to UV light. The application of a photocatalytic coating has been seen in site demonstrations in Belgium [44] and the United States [45,46], along with many others. Abrasion has been known to dislodge TiO_2 from the surface leaving unreactive pieces of pavement [45]. Further studies elucidated the photocatalytic capabilities of the coatings significantly decreased after one month [22].

Experimental Methods

Experimental methods are presented in sequence from preparation of the composite materials, functionalization of the catalyst, cement mixtures and curing, and then assessment of reactivity and longevity. Each step of the procedural methods documented below draws upon the background presented above.

Functionalization of Ti-MAH

Titanium dioxide was originally functionalized to maleic anhydride at ratios of three to one (3Ti-MAH) and two to one (2Ti-MAH), respectively. Ratios listed above were based upon theoretical reactive bonding sites available in the Ti-MAH group, reactive sites of the functionalized material available in order for the group to bind to cementitious media, and finally the minimal amount of titanium required. TiO_2 and MAH were dissolved in methanol in these three ratios and heated until the solution temperature equilibrated to 65° Celsius. Solution maintained a constant temperature for 4 hours and continuously stirred in order to allow for complete functionalization to occur [32]. Solution was then placed in an oven at 35° Celsius or dried in ambient conditions until only powder remained. The resultant powder was ground by mortar and pestle to an equivalent particle gradation. Analysis of the functionalized material was performed using Fourier-transform infrared spectroscopy (FTIR) and x-ray diffraction (XRD) to verify permanent structural bonding.

Materials and Mixture Proportions

In order to test the permanence of bonding within cementitious paste, mixtures were prepared in small batches and placed in containers compliant with ISO testing procedures. Cement paste was mixed using OPC and ASTM grade de-ionized water (DI water) at a water to cement w/c ratio of 0.485. Mixtures included the incorporation of TiO_2 or functionalized TiO_2 by an equivalent weight of cementitious material. Type I/II OPC conforming to ASTM C150/C150M was used with a Blaine fineness of 373 m^2=kg (1; 821 ft^2=lb) and a Bogue composition of 55% C3S, 17% C2S, 8% C3A, and 10% C4AF [47, 48]. Titanium (IV) oxide, Aeroxide ® P25, ACROS Organics was purchased from Thermo Fisher Scientific.

XRD analysis of the P25 indicated the TiO_2 was composed of primarily anatase and some rutile, with anatase presenting more intense peaks. Maleic anhydride (99% purity, Lot#MKCJ0038) was purchased from Sigma Aldrich Company and ACS reagent grade methanol (99.8% purity) was purchased from thermo Fisher Scientific. MAH and Ti-MAH powders were individually sealed in containers which were stored in a desiccator to prevent hydration. The TiO_2 and Ti-MAH were inter-ground by mortar and pestle with the proportioned amounts of cement for their respective mixes (Table 1, 2). The ground powders were all treated as cementitious material with photocatalytic material addition acting as a supplementary cementitious material (SCM). Original testing was performed on 3Ti-MAH with the weight of TiO_2 introduced into the cement at seven percent. However, additional testing was performed on 2Ti-MAH with a varying weight of photocatalytic material after FTIR analysis indicated optimization of the composite could improve reactivity. The water to cement ratio was kept constant for all mixes at 0.485 throughout the original and revised mixing. Mixture proportions for the batches are shown in Table 1 and Table 2 with each batch being mixed and tested in triplicate.

Table 1. Mixture Designs Initial Testing

Mixture	Portland Cement (g)	TiO_2 (g)	3Ti-MAH (g)	DI Water (g)
Control	14.29	-	-	6.93
TiO_2 (7%)	13.29	1.00	-	6.93
3Ti-MAH (7%)	12.96	-	1.33	6.93

Table 2. Mixture Designs Additional Testing

Mixture	Portland Cement (g)	TiO_2 (g)	2Ti-MAH (g)	DI Water (g)
Control	14.29	-	-	6.93
2Ti-MAH (1.5%)	12.96	-	1.33	6.93
2Ti-MAH (7%)	12.79	-	1.5	6.93

Mixing and Curing Procedure

Samples were mixed in transparent borosilicate containers with a diameter of 2-1/8" and height of 2-9/16" for translation to photocatalytic testing described below. (Figure 1). Mixing was performed using hand incorporation of all materials. Each container was vibrated using a vortex mixer set to touch mode for approximately 15 seconds to remove air and to ensure complete mixing. Samples were then placed in a standard environmental chamber set to 100% humidity, 23 °Celsius and allowed to cure for 21 days to ensure complete cement hydration. After initial curing was completed, the samples were placed in an environmental chamber maintained at 50% humidity and 23° Celsius for 7 days to thoroughly dry out for prior to testing.

Photocatalytic Testing

The catalyst reactivity testing procedure was adapted from the International Organization for Standardization standard ISO 10678 [Fine ceramics (advanced ceramics, advanced technical ceramics) – Determination of photocatalytic activity of surfaces in an aqueous medium by degradation of methylene blue] [49]. Methylene blue (MB^+) is an organic chloride salt commonly used to test pollutant reduction capacity in semiconductor photocatalysis because it highlights the efficacy of the photocatalytic process for removal in water pollutants [23]. MB^+ has a high absorptivity and a maximum absorption at a wavelength between 660-665 nm [11, 50, 51]. The features of MB^+ absorption allow for a drastic color change as the compound breaks down into CO_2 and H_2O byproducts [52-54].

35 mL of 10 mg/L methylene blue was pipetted onto the cement and conditioned in a dark room for 12 hours prior to reactivity testing to minimize

adsorption properties of the cement. UVA/B/C lights operating at a range of wavelengths from 550 to 250 nm were precisely placed above the target at a height of 4”. Prior to testing each sample was rinsed in MeOH, followed by DI water to remove lose material and residual dye. 35 mL of 10 mg/L methylene blue was again pipetted onto each cement sample which was then immediately placed under the lamp upon the target. Each sample was irradiated initially for 45 minutes when they were removed from the target. Solutions were extracted from the container and cooled in a darkened container prior to analysis.

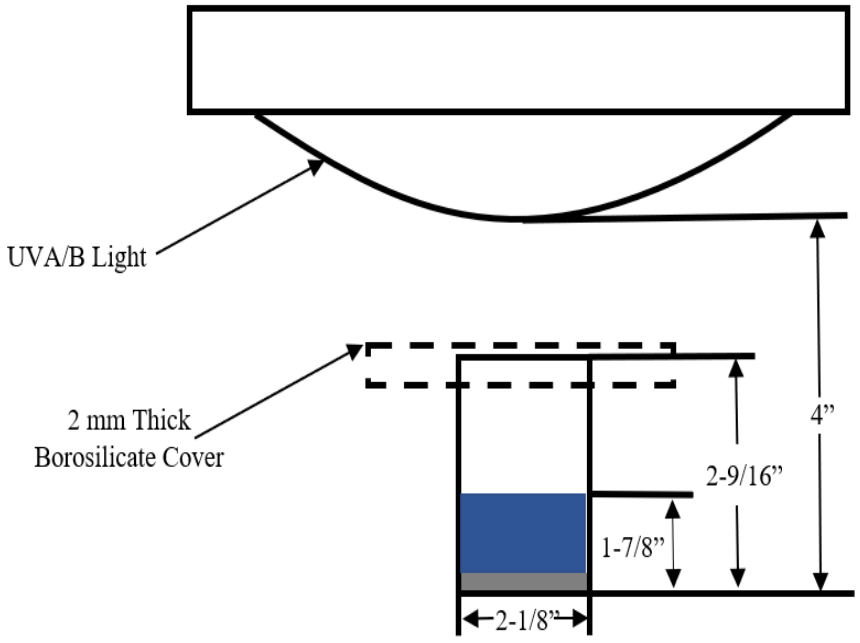

Figure 1 – Photocatalytic Testing Setup

Methylene blue analysis was conducted using a DR3900 Hach UV-Vis Spectrometer and matching quartz cuvettes. Prior to testing calibration of the methylene blue concentrations was performed with a linear relationship achieved between absorption to concentration. Peak wavelength for methylene blue was

measured at 665 nm wavelength with full spectrum analysis performed every three samples. Each absorbance measurement was performed at minimum in triplicate or until variations in values were statistically invariable.

Results and Discussion

Validation of the Functionalization of Ti-MAH

Functionalization of the TiO_2 to MAH was validated using FTIR and XRD. Ti-MAH composites were prepared at a 1:1 ratio for all analysis. FT-IR measurements show a shift and broadening of the carboxylate peaks in the MAH, verifying functionalization (Figure 2). The major structure arrangement from analysis is two C-O-Ti arranged in an open monodentate configuration (Figure 3) [32]. FTIR analysis verified that 3Ti-MAH was not optimal (Figure 2). Therefore, additional photocatalytic testing was performed on using a 2Ti-MAH. The photocatalytic testing discussed later corroborates enhanced reactivity in cement when a 2:1 ratio material is compared to a 3:1, while both are more reactive than TiO_2.

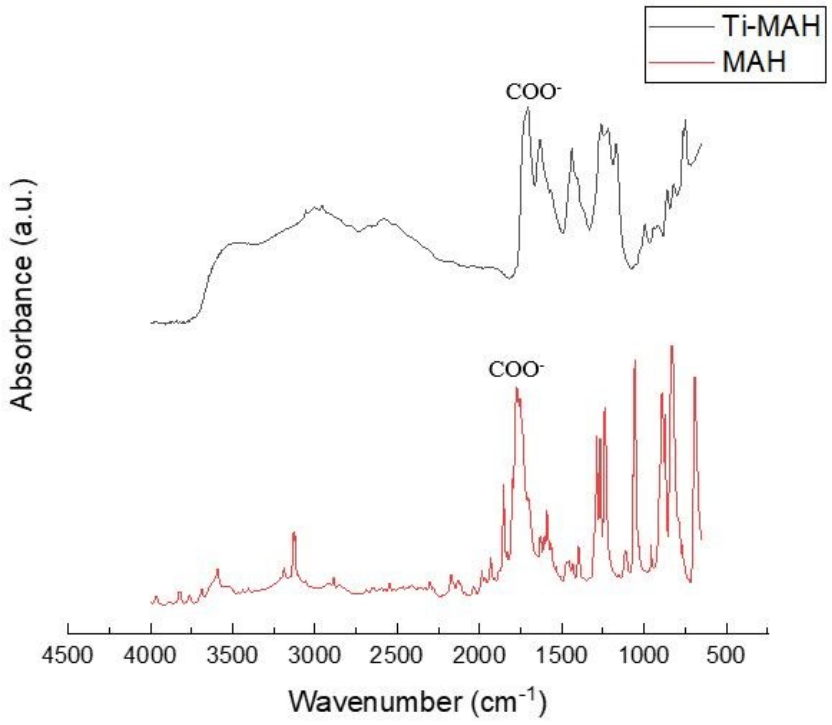

Figure 2 – FTIR Analysis of MAH and Ti-MAH

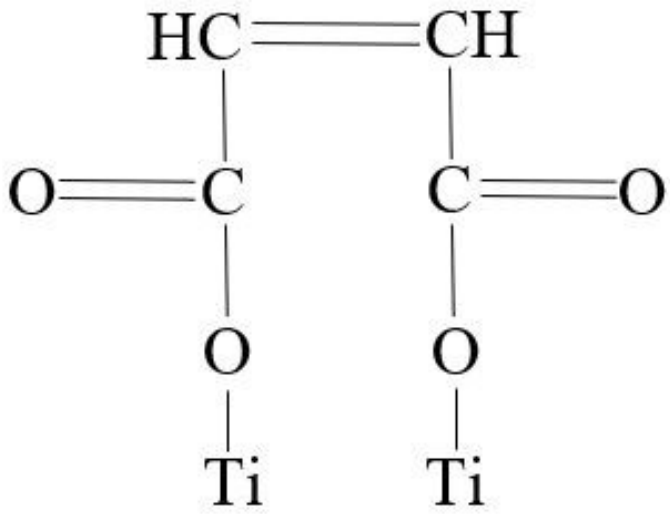

Figure 3 – Proposed Structure Arrangement of 2Ti-MAH

XRD denoted both anatase and rutile peaks with anatase peak intensity being more abundant (Figure 4a). After the TiO_2 was functionalized to the MAH an amorphous structure was detected during XRD analysis starting about 38° and ending

at 58° 2θ angles (Figure 4b). Therefore, indirect evidence of functionalization is present.

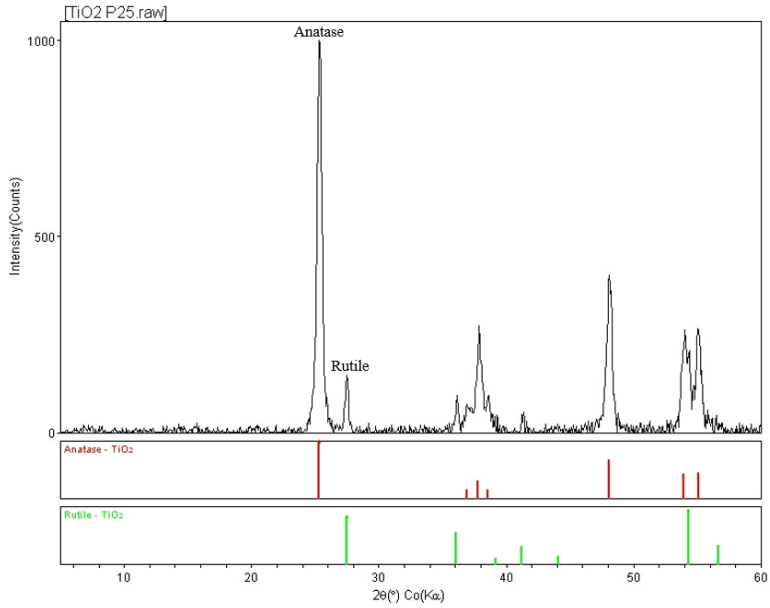

Figure 4a – XRD Diffractogram of P25 Titanium Dioxide

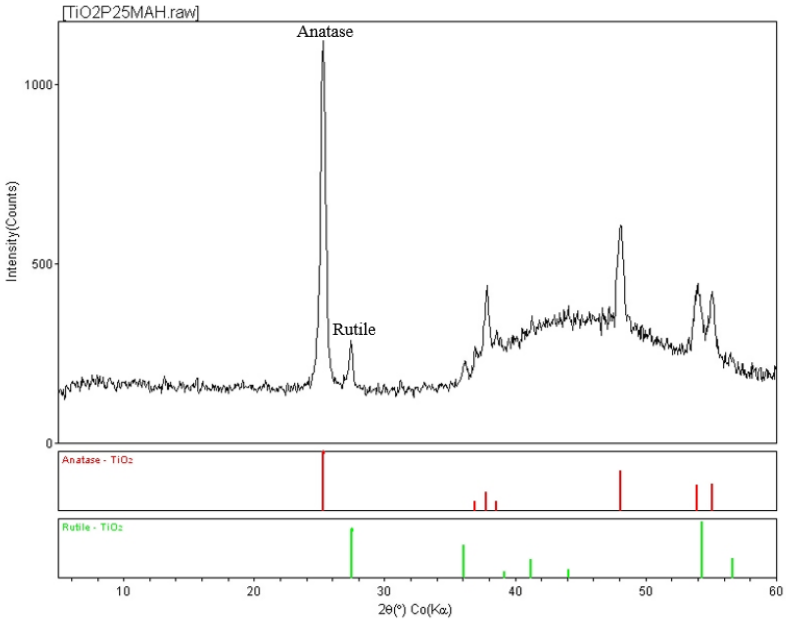

Figure 4b – XRD Diffractogram of Functionalized Ti-MAH Powder

Validation of Ti-MAH Bonding to Silica within OPC

Immobilizing the photocatalysis (TiO_2) within the cement is important to the sustainability and reactivity for continuous treatment. The bonding is theorized to occur in various phases of silicates during cement hydration, specifically calcium-silica-hydrate (C-S-H) gel remains amorphous in structure during cement hydration. During the process of functionalization, the double bond of the maleic anhydride opens up and is fixed onto amorphous silica, similar to manner to grafting the MAH to a polyolefin [55]. In order to verify that functionalized Ti-MAH bonded to C-S-H paste during curing, various, different forms of amorphous surrogate silicas were used to simulate bonding of the various silica phases of cement paste, as well as the point of bonding. This was done in a similar process to the functionalization of the TiO_2 to MAH. Silica was added to methanol at a 1:1 ratio of silica to Ti-MAH. Solutions were continuously stirred for 4 hours after equilibration to promote bonding, to be referred to in this paper as Ti-MAH-Si. The resultant solution was heated at 65 °Celsius and continuously stirred for 12 hours. The Ti-MAH-Si was dried at 35°Celsius for 24 hours and the dried residuals ground to an equivalent gradation using mortar and pestle. FT-IR, XRD, and SEM/EDS analysis was performed on powder from the same batch.

FTIR was performed on Ti-MAH and Ti-MAH-Si to determine bonding points to MAH (Figure 5). The two spectra demonstrate the vibration changes with silica addition. The shift and broadening of MAH carboxylates peaks are still present, while some additional peaks are shown below 1500 cm^{-1}. These vibration changes correlate with the silica spectra and are justified considering the silica addition. The primary

peak of interest, which validates the MAH-Si bond, is the C-H stretch peak. The C-H stretch indicates whether a single bond, double bond, or triple bond is present in the structure. Vibrational peaks of the =C-H stretch in MAH is 3124 cm^{-1} [56].

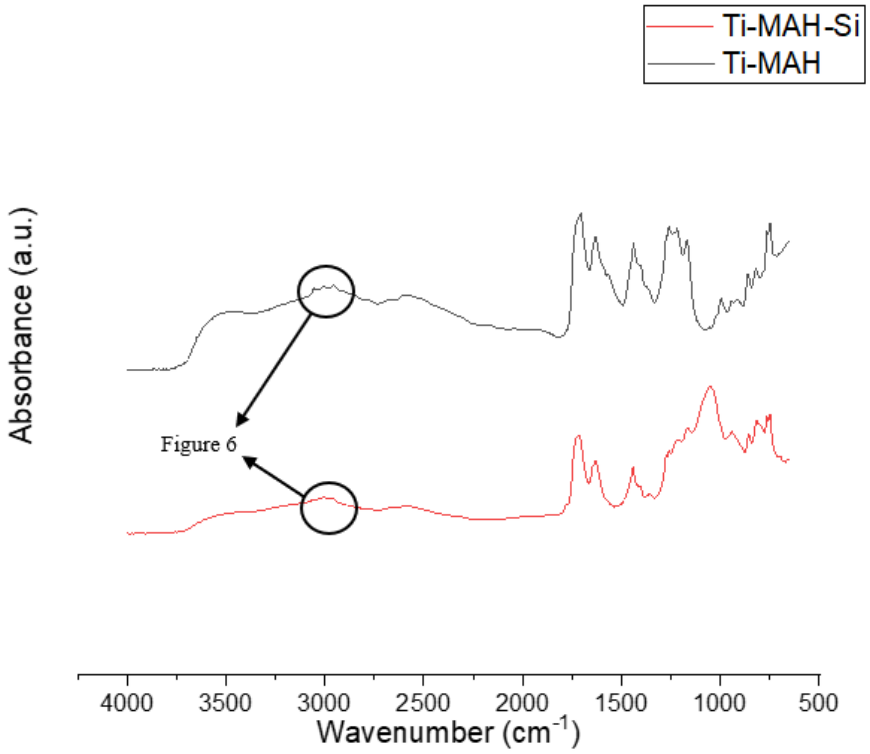

Figure 5 – FTIR Comparison of Ti-MAH and Ti-MAH-Si

Figure 6 shows the =C-H stretch in the Ti-MAH is present. This peak is no longer present in the Ti-MAH-Si spectra seen in Figure 6, which verifies that the double bond breaks to bond silicon to the Ti-MAH. The theorized structures of MAH, 2Ti-MAH, and 2Ti-MAH-Si are presented in Figure 7.

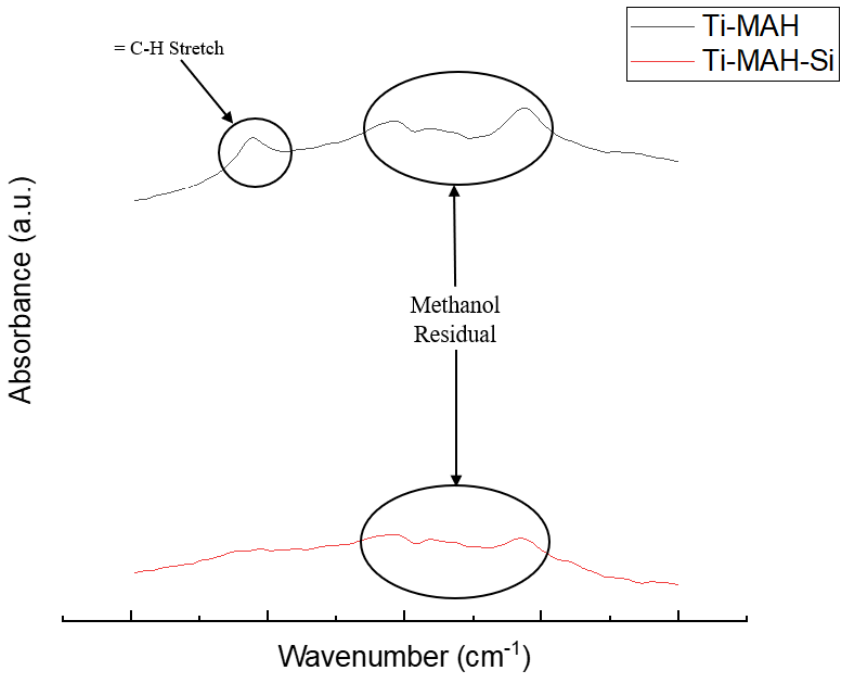

Figure 6 – FTIR Comparison of Ti-MAH and Ti-MAH-Si C-H Stretch.

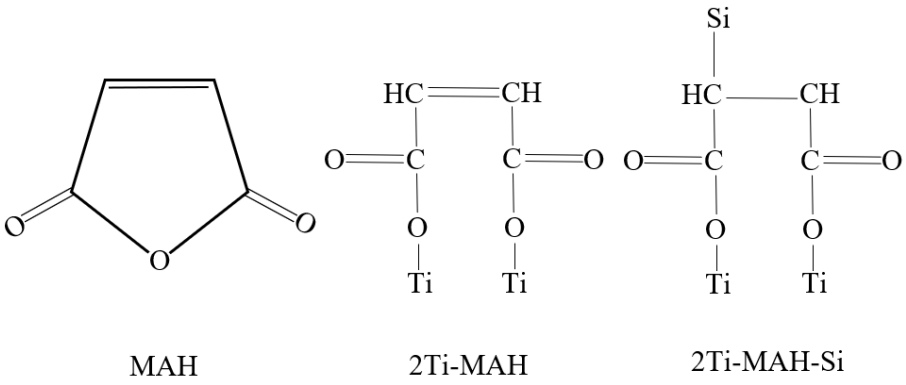

Figure 7 – Proposed Structure Arrangement of MAH, 2Ti-MAH, and 2Ti-MAH-Si

Powders prepared for FTIR were also used for scanning electron microscopy (SEM) analysis. Figure 8 shows a SEM image in backscatter electron mode with energy dispersive x-ray (EDS) used for elemental mapping of ground silica powder that had undergone functionalization. The Ti-MAH particle within the beam focus exhibit extensive coating of the silica particles, showing evidence of the bond to silica.

Some of the rougher surfaces which lack complete coverage are either outside the beam focus or appear to exhibit less TiO_2 bonds. Therefore, the same process was done on a fumed silica (Figure 9), a common supplementary cementitious material.

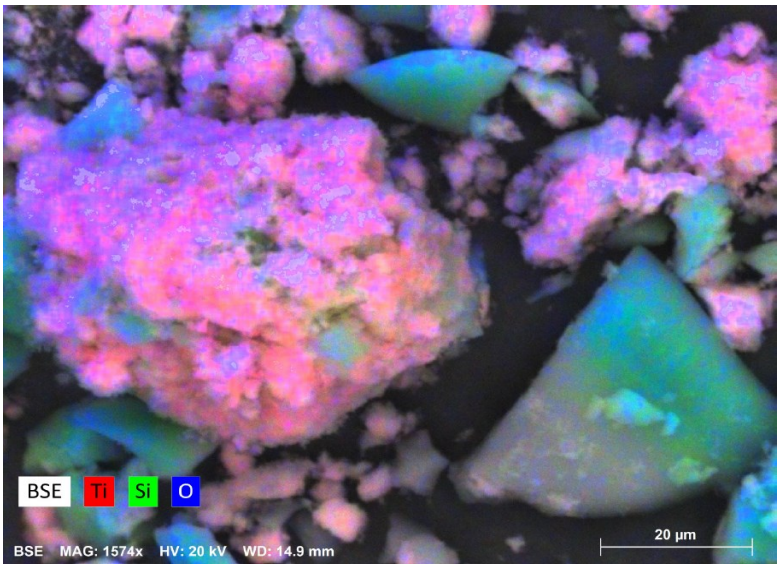

Figure 8 - SEM Backscatter Image with XPS Elemental Mapping (crushed silica)

Note: Silica grains are shown in green hues while titanium is shown in red. The silica grain shown in the beam focus is thoroughly coated on all faces and edges indicating homogenous bonding.

Fumed silica is a nanoparticle synthesized by pyrolysis processes; therefore, it lacks the rough edges present in the ground silica in Figure 8. In comparison, Figure 10 shows the elemental mapping of titanium and silicon functionalized on fumed silica particles. Elemental mapping imagery very clearly indicates that titanium is always present where silicon is present. From this imagery it can be determined the titanium is evenly coating the silica particles. While both images validate TiO_2 coating the silica, the fumed silica has a more homogenous coating which is more correlative to C-S-H gel in cement.

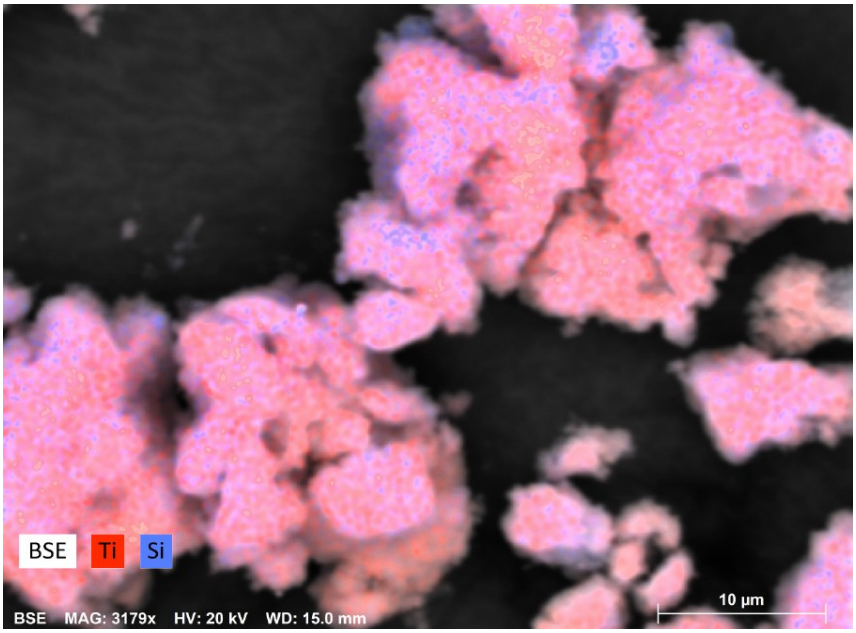

Figure 9 - SEM Backscatter Image with XPS Elemental Mapping (silica fume, overlay)

Note: Silica fume grains are shown in blue hues while titanium is shown in red.

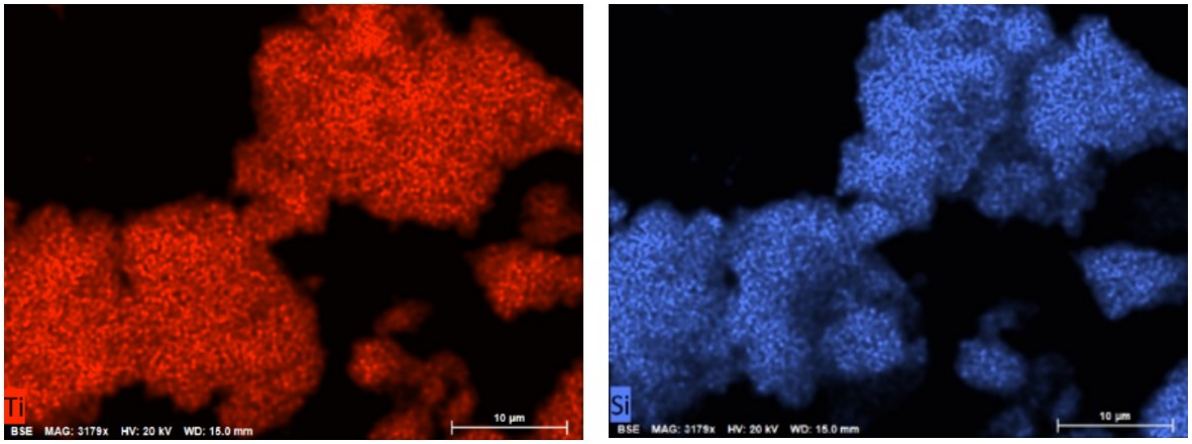

Figure 10 - SEM Backscatter Image with XPS Elemental Mapping (silica fume)

Note: Silica fume grains are shown in blue hues while titanium is shown in red.

The C-S-H phase is the most abundant hydration product of portland cement [57]. C-S-H grows in nanocrystalline structures surrounded by amorphous regions called the interfacial transition zone or ITZ [58]. Theoretical bonding of the Ti-MAH is proposed in the amorphous regions of the C-S-H. In order to support this hypothesis,

Ti-MAH was analyzed within the cement paste by SEM after cyclic testing of reactivity was completed (Figures 11a,b). Imagery shows the Ti-MAH clumped within certain regions of the cement pastes, with the largest clumps averaging 250 microns in width. These clumps act as micro-aggregated TiO_2 within the cement paste.

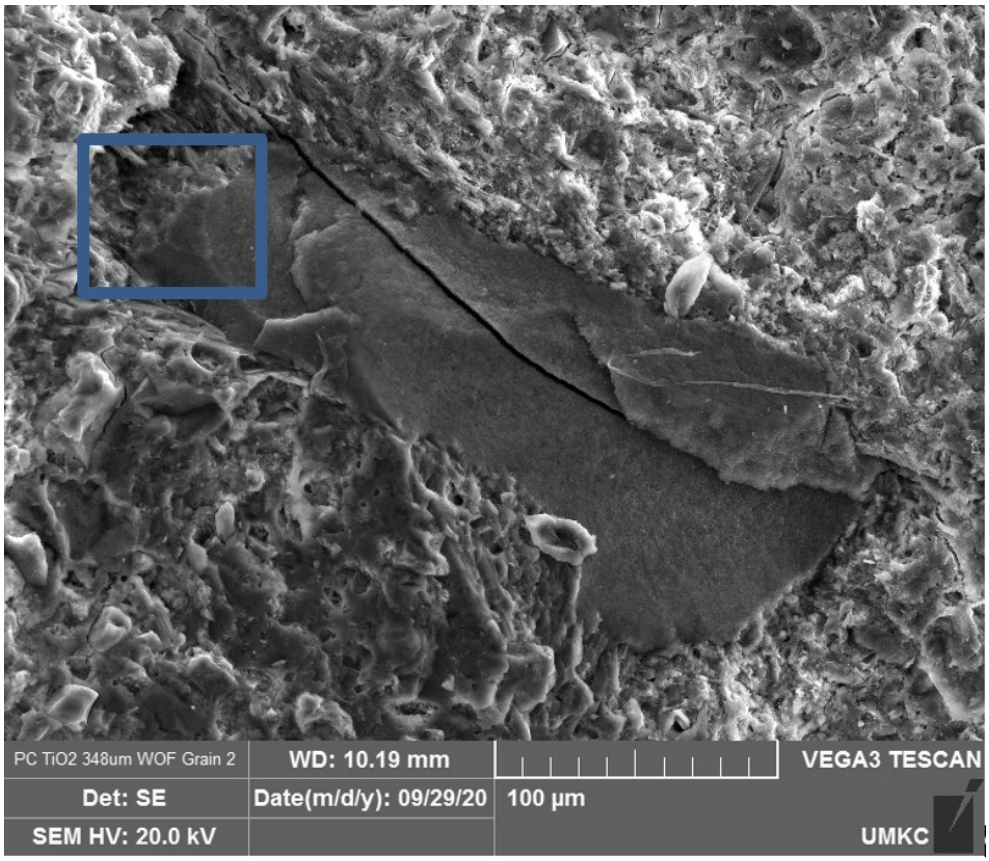

Figure 11a - SEM Secondary Electron Image of TiO_2 Immobilized with the Cement Structure.

Note: the blue box marks the location of image 11b

The heterogenous consistency is theorized to be from the Ti-MAH bonding to the C-S-H. Further analysis along the boundary of the aggregated TiO_2 and the main cement paste composite verified the immobilization of the particles due to bonding within the C-S-H (Figure 11b). Herein, amorphous C-S-H is interlocked to the aggregated TiO_2 with crystals phases growing into the C-S-H substantiating complete immobilization. An interfacial transition zone

(ITZ) is found surrounding the boundary of the aggregate TiO_2 clumps, verifying it is acting as an aggregated particle [59]

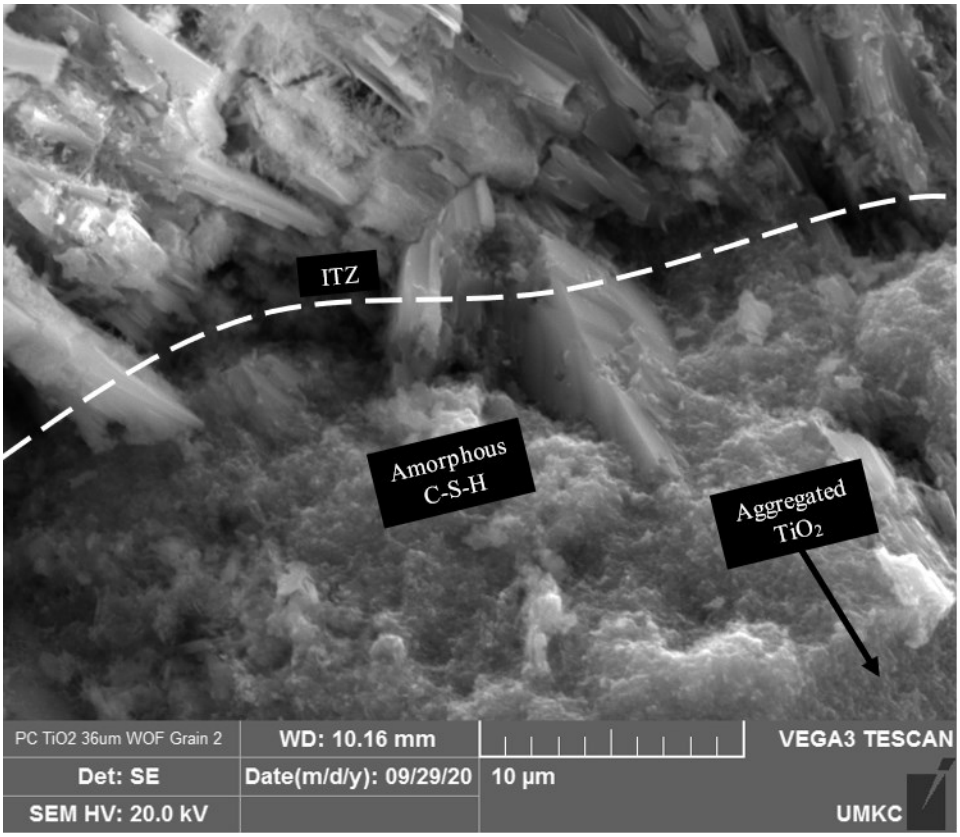

Figure 11b - SEM Secondary Electron Image of the Interlocking of C-S-H and TiO_2 Along the Boundary of the Aggregated TiO_2.

A cross-section was taken from a randomized section of the sample to in order to calculate the average surface area of the TiO_2 remaining after continuous cyclic reactivity testing (Figure 12). The SEM cross section image was converted to a binary threshold in Image J. Surface area of TiO2 within relative to the entire sample cross section was calculated at 6.83% including the aggregated TiO2 as seen in Figure 11a.

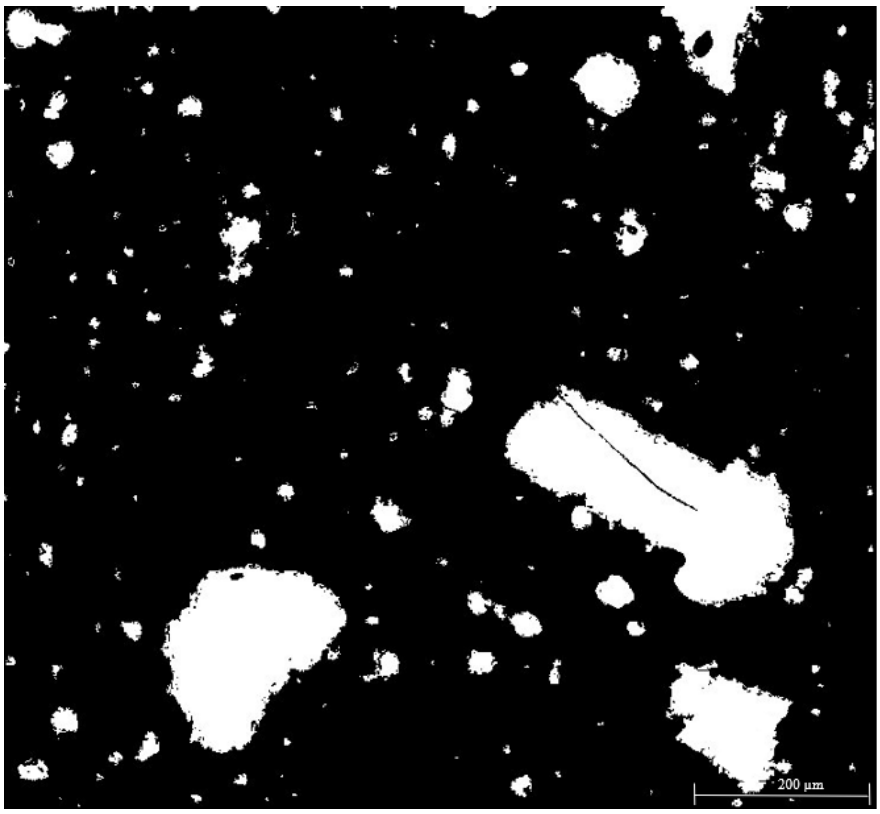

Figure 12 - SEM Backscatter Image Converted to Binary to Calculate an Averaged Surface Area of TiO_2

Titanium nanoparticles are known to act as nucleation sites for cement hydration products that form around the particle. Aggregated TiO_2 is hypothesized to occur as C-S-H gel crystalizes within the pore space and nucleation are occurring. Additionally, maleic acid is a super plasticizer and dispersant which retards the rate of hydration. Retardation of hydration and crystallization of cement paste occurs at a slower pace than nucleation forming ion gradients. Mobile phases such as calcium and aluminum diffuse away from the TiO_2 across the ITZ and form crystalline calcium hydrate structures as seen in Figure 11b. Less mobile phases including the anhydrates and silicates form hydration products near the interfacial zone of aggregated TiO_2 and the rest of the cement paste where amorphous C-S-H forms, containing residual water

from hydration and ion separation. The formation of this ITZ along the anhydrate boundary clearly immobilizes the titanium within the paste while maintaining the theoretical reduced composite band gap of the Ti-MAH structure. Physical immobilization of the Ti-MAH compound within the paste at preferential orientations is only a portion of the analysis as it does not verify improved photocatalytic reactivity relative to TiO2 inter-ground with cement pastes during mixing.

Cyclic Photocatalytic Reactivity Testing of TiO_2 Versus Ti-MAH in Cement

Photocatalytic reactivity testing was first performed on the mixes from Table 1 utilizing the 3Ti-MAH and the ISO standard concentration of 10 mg/L methylene blue. Three repeated cycles of reactivity testing were performed on each batch, in order to compare photocatalytic reactivity of the cement over time and across photocatalysts. Figure 13 presents the results of photocatalytic capacities over cycles. The OPC utilized is a grey cement and therefore is denoted as grey control (GC), while the TiO_2 and 3Ti-MAH mixtures are denoted as such. Each cycle of testing was performed over 45 mins each. The 3Ti-MAH mixture consistently tested more reactive than the grey control and TiO_2 mixture and maintained that reactivity over time which verifies that immobilization of the photocatalyst using the Ti-MAH improves reactivity (Figure 14).

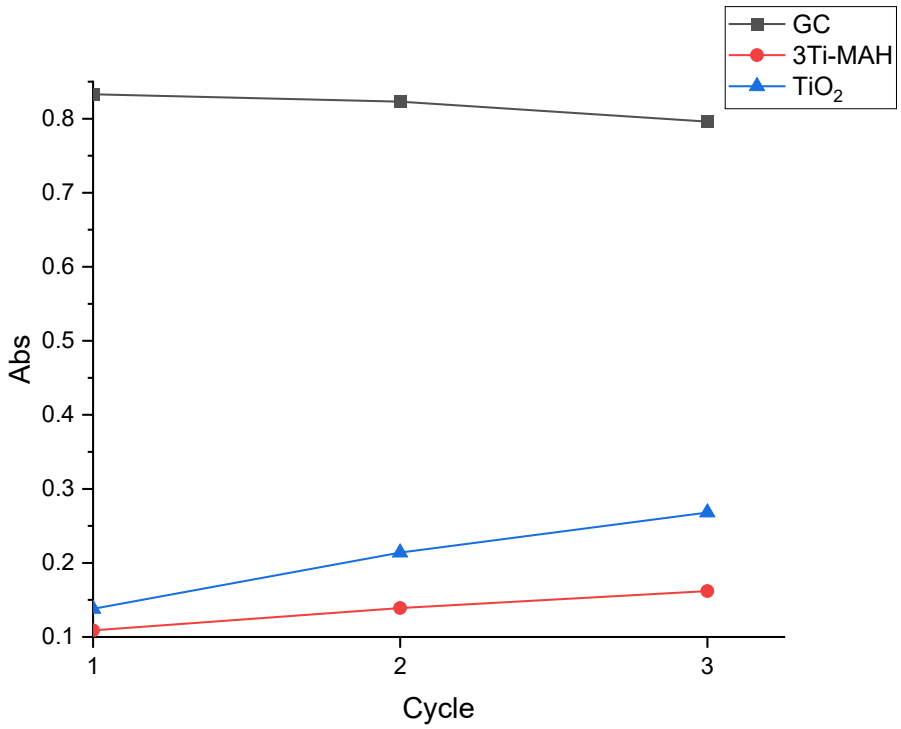

Figure 13 – Results of Photocatalytic Testing of TiO_2 and 3Ti-MAH.

After FT-IR analysis was performed on the Ti-MAH, it was determined that a 2:1 ratio of TiO_2 to MAH could be more reactive. Therefore, additional reactivity testing was done on a 2:1 ratio, however, titanium amounts were varied to include both 1.5%, and 7% TiO_2 by weight of cementitious materials (Table 2). Cycle testing was again conducted to three cycles at 30 minutes instead of 45 minutes to determine if the 2Ti-MAH was more reactive than the 3Ti-MAH. Results indicated the 2Ti-MAH cycled over 30 minutes performed comparably in decomposition rates and concentration of MB^+ as the 3Ti-MAH maintained in 45 minutes. Therefore, the 2Ti-MAH was determined to be a more optimal ratio for reactivity and improved performance.

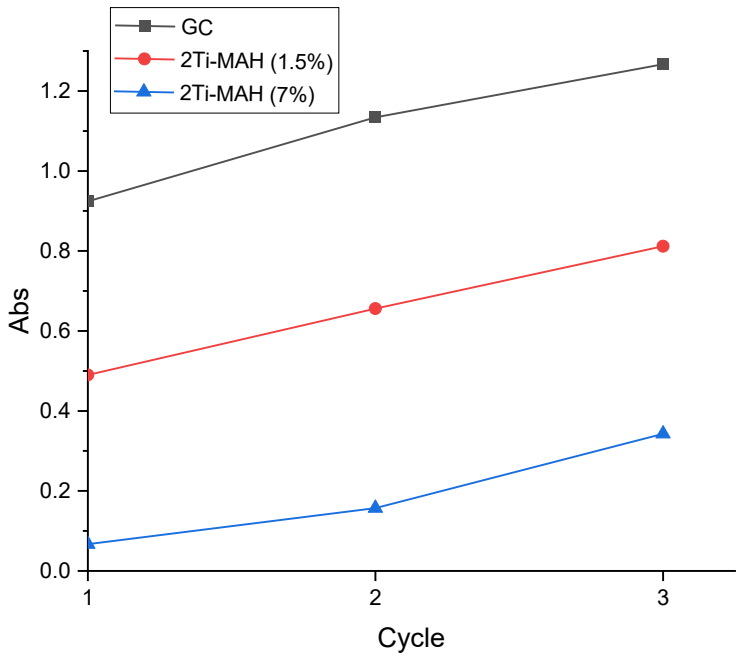

Figure 14 – Abs. Over Cycles Comparison of 2T-iMAH (7%) and 2Ti-MAH (5%)

Stability of MB^+ in Photocatalytic Testing

The rates of decomposition of MB^+ must be evaluated as function of MB^+ concentration, mass of TiO2, and pH of solution as MB^+ decomposition is highly pH dependent. High pH or alkaline solutions react with methylene blue, a cationic thiazine dye, resulting in the decay of MB^+ and the formation of methylene violet Brenthsen when solution pH rises above 9.0 S/U [23]. The rate of MB^+ decomposition is dependent upon the concentration of hydroxyls in solution as well as the dye itself. Methylene violet is essentially a hydrolysis decomposition product that may decay further under sustained alkaline conditions. Therefore, it is necessary to validate the use of MB^+ as an indicator of photocatalytic abilities on cement paste as solutions directly in contact with the wetted surface of fresh cements may experience sustained, highly alkaline conditions [60]. Excess hydroxyls from the hydration process such as

calcium hydroxide are held in cement pores until flushed [61]. During flushing of the pores, free hydroxyls diffuse out into free solution, over time raising the pH of aqueous solutions immediately in contact with the wetted cement surface.

The pH of the initial 10mg/L MB^+ solution was approximately 8 to 8.2 S/U. After each cycle, the treated solutions were measured to determine if a correlation of pH to reactivity or MB^+ decay was present in the experimental design. During the first cycle, the pH of the control grey cement, GC, was over 11.0 S/U. However, with each iterative cycle, the pH of the solutions decreased until such time as there was no appreciable difference from initial to final pH, occurring at the end of cycle 3. This implies a nucleophile attack on the MB^+ from the excess hydroxyls freed during flushing of the cement in the form of $Ca(OH)_2$, could be occurring in the initial cycles. As the presence of excess hydroxyls in solutions decreases, the nucleophile attack decreases, which functions to increase the initial decomposition rate of the MB^+ compound relative to the final measurement. Each sample possessed the same water to cement ratio and weight of cementitious material. Therefore, each sample must also possess the same number of excess hydroxyls released into solution, and hence the nucleophile attack must cease by the third cycle for all samples.

If nucleophile attack has ceased by the third cycle, the difference in performance between each sample mixture must be attributable to photocatalytic degradation of the MB^+. Indeed, photocatalytic degradation of MB^+ should result in the formation of sulfuric acid and carbon dioxide gas. The sulfuric acid may be neutralized by the buffering capacity of the cement itself until the cement lacks mitigating capacity. Carbon dioxide gas reacts with the cement to form calcium

carbonate, reducing the overall pH and making the cement more prone to sulfate attack. The point at which excess hydroxyls are no longer freed by aqueous solution is commonly considered the carbonation point of the cement or concrete material. SEM (Figures 11a,b) imagery confirms the lack of portlandite in the samples after continuous cycle testing in the GC control and thus validates that nucleophile attack has ceased.

In an effort to further validate that functionalization is the primary reason for the improved reactivity of the Ti-MAH samples, Hydrion One Drop 1.0-11.0 indicator solution was applied to the top face, bottom face, and a broken cross-section of a 2Ti-MAH sample (Figure 15). Surface dying with phenolphthalein is commonly performed to assess the rate and/or point at which carbonation of cement occurs [62]. However, phenolphthalein would not show the range of pH of a cement sample with distance from an exposed surface and requires an uncarbonated control sample. Indicator dye verified that pH within the cement sample increased with distance from the surface exposed to MB^+ solutions during treatment. Surfaces directly exposed to the MB^+ solution during cycles are dyed yellowish orange, indicating a pH of approximately 6 S/U. As distances increases from the treatment surface, dye coloration exhibits a color ramp or gradient from light grayish blue to intense purple, representing a rise in pH above 11 S/U. The cross section further validates that pH had reduced below 8.0 pH in the Ti-MAH and that the difference in performance is from the enhance reactivity due to functionalization.

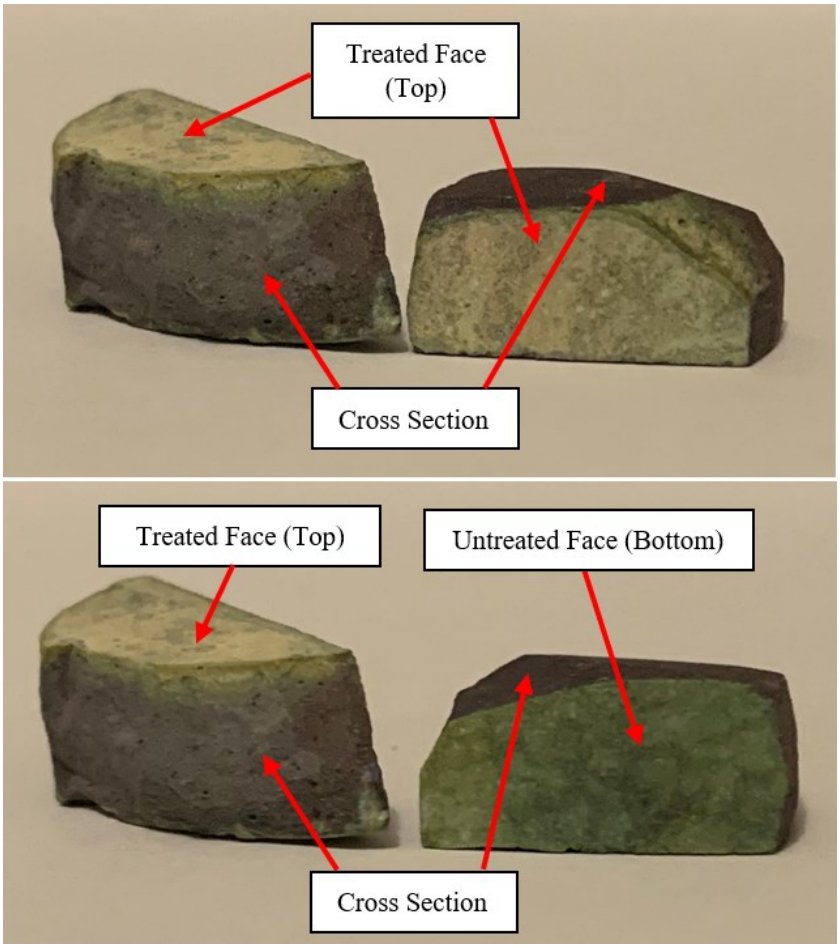

Figure 15 – pH of 2Ti-MAH Sample After Cycle Testing

Photocatalytic Capabilities of 2Ti-MAH in White Cement Versus Commercially Available Cement

While the increased reactivity of 2Ti-MAH compared to TiO_2 was demonstrated in trials utilizing grey cement, additional testing was performed using white cement to compare against a commercially available photocatalytic cement. The exact percent of TiO_2 in the commercially available cement is unknown, however, is estimated to be approximately 5-8%. Therefore, the 2Ti-MAH was inter-ground with a white cement base from the same source as the commercially photocatalytic available cement. Four 30-minute cycles were performed as shown in Figure 16. Similar slopes are seen in cycles 1-3, with 2Ti-MAH being more reactive

and retaining a greater degradation percent. Between cycles 3 and 4 the commercially available photocatalytic cement decreases in efficiency by more than two times that of the 2Ti-MAH. 2Ti-MAH remains equally as reactive as the cycle before. Results validates using 2Ti-MAH is a superior process for the development of photocatalytic cement.

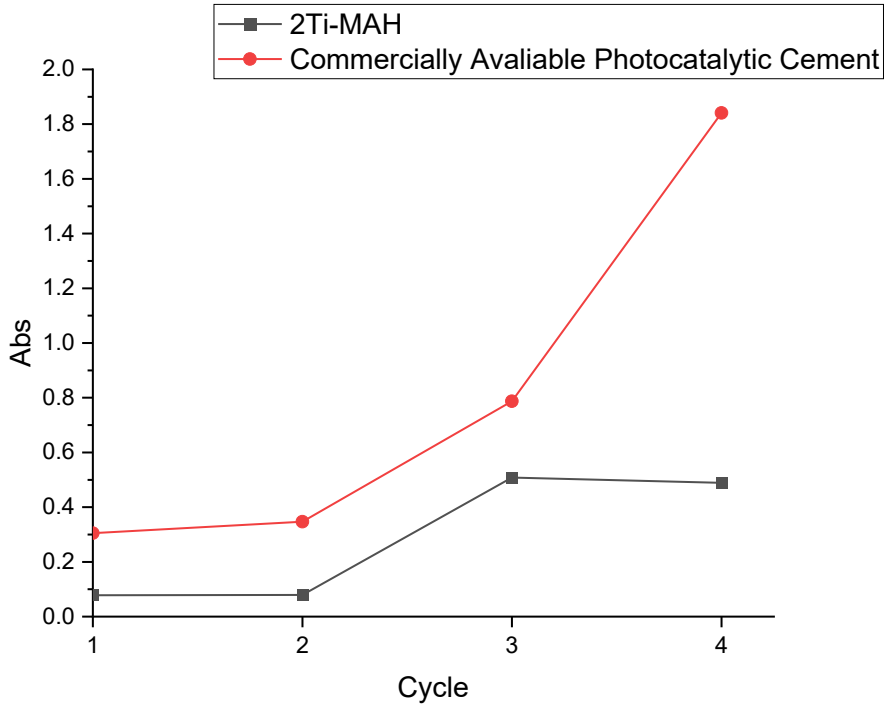

Figure 16 – Abs Over Cycles, Comparison of 2Ti-MAH Versus Commercially Available Photocatalytic Cement

Applications

Functionalizing the titanium enables the permanent bond to amorphous silica, essentially making almost any amorphous silica photocatalytic. The uses for titanium immobilized in this matter go beyond photocatalytic concrete and includes paints, ceramics, glass, coatings, dyes, crayons, sunscreen, varnishes, and paper products. Finally, immobilization of the titanium in the Ti-MAH-Si structure prevents

nanoparticle dispersion in the environment making this a more sustainable choice for treatment techniques.

Conclusion

Silica was bonded to photocatalytic titanium using the simple and efficient procedure of bridge the two with maleic anhydride (MAH). Bonding the Ti-MAH-Si together allowed for optimal orientation of the titanium particles within the silicon. Multiple robust lines of evidence were used to verify the bond formation between Ti-MAH and silica. For each iteration, ratio adjustments of Ti to MAH or mass of titanium within the cement samples were tested to determine bond strength, reactivity, and longevity of reactivity. The optimal ratio for enhanced reactivity performance was found to be a 2:1 ratio of TiO_2:MAH. Additionally, when Ti-MAH is bonded within the cement pastes were cycled, the resulted clearly delineate increased reduction of methylene blue (MB^+) concentration over time and improved longevity of cement pastes. Using effectively orientated and functionalized titanium within cement has great potential to enhance photocatalytic capacities of concrete and therefore improve treatment of non-point and point sources of organic contaminants. If the photocatalytic cement were used as a granular filter of media, enhanced organic removal capacity would occur considering free radicals would generate over more surface area with more contact time. Furthermore, cement is only one use for bonding Ti-MAH to silicon as there are many applications of use which could include paints, coatings and adhesives, construction building materials, and plastic modifiers. Given the potential uses, ease of preparation and application, and enhancement of performance over time, this technique is a promising means for reducing organic contaminants in air or water.

References

[1] Brown, J. N. (2002). Partitioning of Chemical Contaminants in Urban Stormwater (Thesis, Doctor of Philosophy). University of Otago.

[2] Foster, G. D., Roberts, E. C., Gruessner, B., & Velinsky, D. J. (2000). Hydrogeochemistry and transport of organic contaminants in an urban watershed of Chesapeake Bay (USA). *Applied Geochemistry*, *15*(7), 901–915. https://doi.org/10.1016/S0883-2927(99)00107-9

[3] ITRC (Interstate Technology & Regulatory Council). (2020). PFAS Technical and Regulatory Guidance Document and Fact Sheets PFAS-1. *Washington, D.C.: Interstate Technology & Regulatory Council, PFAS Team*. https://pfas-1.itrcweb.org/.

[4] Mahlambi, M. M., Ngila, C. J., & Mamba, B. B. (2015). Recent Developments in Environmental Photocatalytic Degradation of Organic Pollutants: The Case of Titanium Dioxide Nanoparticles-A Review. *Journal of Nanomaterials*, *2015*. https://doi.org/10.1155/2015/790173

[5] Spatari, S., Yu, Z., & Montalto, F. A. (2011). Life cycle implications of urban green infrastructure. *Environmental Pollution*, *159*(8–9), 2174–2179. https://doi.org/10.1016/j.envpol.2011.01.015

[6] Brown, R. A., Asce, A. M., & Borst, M. (2014). *Evaluation of Surface Infiltration Testing Procedures in Permeable Pavement Systems*. *140*(3), 1–12. https://doi.org/10.1061/(ASCE)EE.1943-7870.0000808

[7] Welker, Andrea L., James D. Barbis, and Patrick A. Jeffers. (2012). A Side-by-Side Comparison of Pervious Concrete and Porous Asphalt. *Journal of the American Water Resources Association* (JAWRA) 48(4): 809-819. DOI: 10.1111/j.1752-1688.2012.00654

[8] Asadi, S., Hassan, M., Kevern, J., & Rupnow, T. (2012). Development of photocatalytic pervious concrete pavement for air and storm water improvements. *Transportation Research Record*, *1972*(2290), 161–167. https://doi.org/10.3141/2290-21

[9] Kayhanian, M., Li, H., Harvey, J. T., & Liang, X. (2019). Application of permeable pavements in highways for stormwater runoff management and pollution prevention: California research experiences. *International Journal of Transportation Science and Technology*, *8*(4), 358–372. https://doi.org/10.1016/j.ijtst.2019.01.001

[10] Monrose, J., & Tota-Maharaj, K. (2016). *Permeable Pavements as Low Impact Development Practices for Urban Runoff Mitigation and Sustainable Stormwater Management within the Built Environment for the Caribbean*. *October 2016*, 24–28.

[11] Spahr, S., Teixidó, M., Sedlak, D. L., & Luthy, R. G. (2020). Hydrophilic trace organic contaminants in urban stormwater: Occurrence, toxicological relevance, and the need to enhance green stormwater infrastructure. *Environmental Science: Water Research and Technology*, *6*(1), 15–44. https://doi.org/10.1039/c9ew00674e

[12] Environmental Protection Agency (EPA), Office of Water (1999) Preliminary Data Summary of Urban Storm Water Best Management Practices, EPA-821-R-99-012

[13] Todd, G., Chessin, R., Colman, J. (1999). Toxicological Profile for Total Petroleum Hydrocarbons (TPH). *Agency for Toxic Substances and Disease Registry.*

[14] Björklund, K. (2011). Sources and Fluxes of Organic Contaminants in Urban Runoff (Thesis, Doctor of Philosophy). Chalmers University of Technology.

[15] Mangiafico, S. S., Newman, J., Merhaut, D. J., Gan, J., Faber, B., & Wu, L. (2009). Nutrients and Pesticides in Stormwater Runoff and Soil Water in Production Nurseries and Citrus and Avocado Groves in California. *HortTechnology,* 19(2), 260-367. https://doi.org/10.21273/HORTSCI.19.2.360

[16] Ellis, J. B. (2006). Pharmaceutical and personal care products (PPCPs) in urban receiving waters. *Environmental Pollution*, *144*(1), 184–189. https://doi.org/10.1016/j.envpol.2005.12.018

[17] Xiao, F., Simcik, M. F., & Gulliver, J. S. (2012). Perfluoroalkyl acids in urban stormwater runoff: Influence of land use. *Water Research*, *46*(20), 6601–6608. https://doi.org/10.1016/j.watres.2011.11.029

[18] Codling, G., Yuan, H., Jones, P. D., Giesy, J. P., & Hecker, M. (2020). Metals and PFAS in stormwater and surface runoff in a semi-arid Canadian city subject to large variations in temperature among seasons. *Environmental Science and Pollution Research*, *27*(15), 18232–18241. https://doi.org/10.1007/s11356-020-08070-2

[19] Hassaan, M. A., & Nemr, A. El. (2017). Health and Environmental Impacts of Dyes : Mini Review. *American Journal of Environmental Science and Engineering*, *1*(3), 64–67. https://doi.org/10.11648/j.ajese.20170103.11

[20] Raval, N. P., Shah, P. U., & Shah, N. K. (2016). Malachite green 'a cationic dye' and its removal from aqueous solution by adsorption. *Applied Water Science*. https://doi.org/10.1007/s13201-016-0512-2

[21] Delnavaz, M , Ayati, B., Ganjidoust H., & Sanjabi S. (2012) Kinetics study of photocatalytic process for treatment of phenolic wastewater by TiO_2 nano powder immobilized on concrete surfaces, *Toxicological & Environmental Chemistry*, 94:6, 1086-1098, DOI: 10.1080/02772248.2012.688331

[22] Osborn, D., Hassan, M., Asce, M., Asadi, S., & White, J. R. (2014). *Durability Quantification of TiO 2 Surface Coating on Concrete and Asphalt Pavements*. *x*, 331–337. https://doi.org/10.1061/(ASCE)MT.1943-5533.0000816.

[23] Mills, A., Hazafy, D., Parkinson, J., Tuttle, T., & Hutchings, M. G. (2011). Effect of alkali on methylene blue (C.I. Basic Blue 9) and other thiazine dyes. *Dyes and Pigments*, *88*(2), 149–155. https://doi.org/10.1016/j.dyepig.2010.05.015

[24] Fujishima, A., T. N. Rao, and D. A. Tryk (2000). Titanium Dioxide Photocatalysis. *Journal of Photochemistry Reviews,* Vol. 1, pp. 1–21.

[25] Khan, M. M., Adil, S. F., & Al-Mayouf, A. (2015). Metal oxides as photocatalysts. *Journal of Saudi Chemical Society*, *19*(5), 462–464. https://doi.org/10.1016/j.jscs.2015.04.003

[26] Martha, S., Chandra Sahoo, P., & Parida, K. M. (2015). An overview on visible light responsive metal oxide based photocatalysts for hydrogen energy production. *RSC Advances*, *5*(76), 61535–61553. https://doi.org/10.1039/c5ra11682a

[27] Fujishima, A., and K. Honda (1972). Electrochemical Photolysis of Water at a Semiconductor Electrode. *Nature,* Vol. 238, pp. 37–38.

[28] Grande F, Tucci P (2016). Titanium Dioxide Nanoparticles: a Risk for Human Health? Mini Rev Med Chem. 16(9):762-9. doi: 10.2174/1389557516666160321114341. PMID: 26996620.

[29] Poulopoulos SG, Yerkinova A, Ulykbanova G, Inglezakis VJ (2019) Photocatalytic treatment of organic pollutants in a synthetic wastewater using UV light and combinations of TiO_2, H_2O_2 and Fe(III). PLoS ONE 14(5): e0216745. https://doi.org/10.1371/journal.pone.0216745

[30] Khdary, N.H.; Alkhuraiji, W.S.; Sakthivel, T.S.; Khdary, D.N.; Salam, M.A.; Alshihri, S.; Al-Mayman, S.I.; Seal, S. (2020). Synthesis of Superior Visible-Light-Driven Nanophotocatalyst Using High Surface Area TiO_2 Nanoparticles Decorated with Cu_xO Particles. *Catalysts,* 10(872). https://doi.org/10.3390/catal10080872

[31] Luttrell, T., & Halpegamage, S. (2014). *Why is Anatase a Better Photocatalyst Than Rutile? - Model Studies on Epitaxial TiO2 Films*. *February*. https://doi.org/10.1038/srep04043

[32] Del Castillo, P. C. H., Manuel, S. R., & Ruiz, F. (2014). An Easy and Efficient Method to Functionalize Titanium Dioxide Nanoparticles with Maleic Anhydride. *Soft Nanoscience Letters*, *04*(03), 53–62. https://doi.org/10.4236/snl.2014.43008

[33] Umar, M. and H. A. Aziz. (2013). Photocatalytic Degradation of Organic Pollutants in Water. *IntechOpen.* DOI: 10.5772/53699

[34] Chong, M. N., Jin, B., Chow, C. W. K., & Saint, C. (2010). Recent developments in photocatalytic water treatment technology: A review. *Water Research*, *44*(10), 2997–3027. https://doi.org/10.1016/j.watres.2010.02.039

[35] Yang, G. C. C., & Li, C. (2007). *Electrofiltration of silica nanoparticle-containing wastewater using tubular ceramic membranes*. *December 2007*. https://doi.org/10.1016/j.seppur.2007.07.019

[36] Alalm, M.G., Tawfik, A., Ookawara, S. (2016) Enhancement of photocatalytic activity of TiO2 by immobilization on activated carbon for degradation of pharmaceuticals, *Journal of Environmental Chemical Engineering*, 4:2, p.1929-1937, ISSN 2213-3437, https://doi.org/10.1016/j.jece.2016.03.023

[37] Laurance, J. (2016). Photocatalytic Treatment of Stormwater Runoff using Puralytics LilyPad (Thesis). Oregon State University.

[38] Mustapha, S., Ndamitso, M. M., Abdulkareem, A. S., Tijani, J. O., & Ajala, D. T. S. A. O. (2020). Application of TiO 2 and ZnO nanoparticles immobilized on clay in wastewater treatment: a review. In *Applied Water Science*. Springer International Publishing. https://doi.org/10.1007/s13201-019-1138-y

[39] Doudrick, K., Monzón, O., Mangonon, A., Hristovski, K., & Westerhoff, P. (2012). Nitrate reduction in water using commercial titanium dioxide photocatalysts (P25, P90, and Hombikat UV100). *Journal of Environmental Engineering (United States)*, *138*(8), 852–861. https://doi.org/10.1061/(ASCE)EE.1943-7870.0000529

[40] Zhao, C., Wang, Z., Wang, C., Li, X., & Wang, C. C. (2018). Photocatalytic degradation of DOM in urban stormwater runoff with TiO2 nanoparticles under UV light irradiation: EEM-PARAFAC analysis and influence of co-existing inorganic ions. *Environmental Pollution*, *243*(December), 177–188. https://doi.org/10.1016/j.envpol.2018.08.062

[41] Cassar, L. & Beeldens, Anne & Pimpinelli, N. & Guerrini, Gian Luca. (2007). Photocatalysis of cementitious materials. *International RILEM Symposium on Photocatalysis, Environment and Construction Materials.* 131-145.

[42] Cackler, T., Alleman, J., Kevern, J., & Sikkema, J. (2012). Environmental Impact Benefits with "TX Active" Concrete Pavement in Missouri DOT Two-Lift Highway Construction Demonstration. Iowa State University.

[43] Yang, L., Hakki, A., Wang, F., & Macphee, D. E. (2018). *Applied Catalysis B: Environmental Photocatalyst efficiencies in concrete technology: The effect of photocatalyst placement*. *222*, 200–208. https://doi.org/10.1016/j.apcatb.2017.10.013

[44] Boonen, E., & Beeldens, A. (2014). *Recent Photocatalytic Applications for Air Purification in Belgium*. *2005*, 553–573. https://doi.org/10.3390/coatings4030553

[45] Shen, S., Burton, M., Jobson, B., & Haselbach, L. (2012). Pervious concrete with titanium dioxide as a photocatalyst compound for a greener urban road environment. *Construction and Building Materials*, *35*, 874-883. https://doi.org/10.1016/j.conbuildmat.2012.04.097

[46] Crain, N., Mcdonald-buller, E., Crain, N., Juenger, M., Cros, C., Terpeluk, A., Burris, L., Mcdonald-buller, E., Sullivan, D., & Street, G. (2017). Laboratory and Field Studies of Photocatalytic NOx and O3 Removal by Coatings on Concrete. The University of Texas at Austin.

[47] ASTM. (2016). "Standard specification for portland cement." *ASTM C150/C150M-16e1*, West Conshohocken, PA.

[48] Cao, Q., and Kevern, J. T. (2015). "Using drinking water treatment waste as a low-cost internal curing agent for concrete." *ACI Mater. J.*, 112(1), 69–77.

[49] ISO 8894-2. (2006). International Standard International Standard. 61010-1 © Iec:2001, 2006, 13.

[50] Milošević, M. D., Logar, M. M., Poharc-Logar, A. V., & Jakšić, N. L. (2013). Orientation and Optical Polarized Spectra (380–900 nm) of Methylene Blue Crystals on a Glass Surface. *International Journal of Spectroscopy*, *2013*, 1–6. https://doi.org/10.1155/2013/923739

[51] Dariani, R. S., Esmaeili, A., Mortezaali, A., & Dehghanpour, S. (2016). Photocatalytic reaction and degradation of methylene blue on TiO2 nano-sized particles. *Optik*, *127*(18), 7143–7154. https://doi.org/10.1016/j.ijleo.2016.04.026

[52] Hou, C., Hu, B., & Zhu, J. (2018). Photocatalytic degradation of methylene blue over TiO2 pretreated with varying concentrations of NaOH. *Catalysts*, *8*(12). https://doi.org/10.3390/catal8120575

[53] Li, R., Jia, Y., Bu, N., Wu, J., & Zhen, Q. (2015). Photocatalytic degradation of methyl blue using Fe2O3/TiO2 composite ceramics. *Journal of Alloys and Compounds*, *643*, 88–93. https://doi.org/10.1016/j.jallcom.2015.03.266

[54] Xu, C., Rangaiah, G. P., & Zhao, X. S. (2014). Photocatalytic degradation of methylene blue by titanium dioxide: Experimental and modeling study. *Industrial and Engineering Chemistry Research*, *53*(38), 14641–14649. https://doi.org/10.1021/ie502367x

[55] Samay, G., Nagy, T. and White, J.L. (1995), Grafting maleic anhydride and comonomers onto polyethylene. J. Appl. Polym. Sci., 56: 1423-1433. doi:10.1002/app.1995.070561105

[56] Layman, A. (1963). A study of the polarized infrared spectrum of maleic anhydride (Doctor of Philosophy in Chemistry). Montana State University.

[57] Lea's Chemistry of Cement and Concrete edited by Beaudoin, J., Odler, I. (Fifth Edition), Butterworth-Heinemann 2019

[58] Science and Technology of Concrete Admixtures, edited by Marchon, D., Flatt, R.J., Elsevier Science, 2015.

[59] Nicolas, R. S., & Provis, J. L. (2015). *The interfacial Transition Zone in alkali-activated slag Mortars*. *2*(December), 1–11. https://doi.org/10.3389/fmats.2015.00070

[60] Grubb, J., Limaye, H., & Kakade, A. (2007). Testing pH of Concrete: Need for a Standard Procedure. *Concrete International*, *29*(4), 78–83.

[61] Hansen, K. (2015). Cement Hydration Kinetics. *National Precast Concrete Association.* https://precast.org/2016/03/cement-hydration-kinetics/

[62] Lo, Y., & Lee, H. M. (2002). Curing effects on carbonation of concrete using a phenolphthalein indicator and Fourier-transform infrared spectroscopy. *Building and Environment*, *37*(5), 507–514. https://doi.org/10.1016/S0360-1323(01)00052-X

CHAPTER 3

PHOTOCATALYTIC POROUS SILICA-BASED GRANULAR MEDIA FOR ORGANIC POLLUTANT DEGRADATION IN INDUSTRIAL WASTE-STREAMS

Introduction

As expansions in the textile industry continue, remedial technologies for textile dyes have become very important and in demand [1]. Since the industrial switch from natural dyes to synthetic, over 100,000 synthetic dyes have been produced and are widely associated with water pollution stemming from the discharge of untreated effluents into bodies of water [2–4]. With no requirement for pretreatment of effluent streams, 280,000 tons of dyes per year are discharged as effluent to water ways [5]. Organic dyes contribute to wastewater in various other aspects such as in hair dye [6] leather and paper industries [7], and luminescent solar concentrator (LSC) technologies [8]. Organic chemicals used in dyes are known to be toxic to the environment and cause detrimental health effects in humans, such as respiratory illnesses [9]. Textile dyes are highly soluble, organic compounds that cannot be effectively treated using conventional wastewater treatment technologies. Dye-specific treatment methods include adsorption and electro-chemical destabilization; however, these processes produce concentrated waste streams or additional byproducts which require further treatment or disposal [10]. Degradation of textile dyes by nucleophilic attack has been shown to be a promising method for mineralization of methylene blue as individual components [11,12]. Photocatalytic degradation processes have also shown to be effective in rapidly degrading numerous organic pollutants, including textile dyes [13,14]. Very few existing technologies combine the attacks for an improved treatment.

Photocatalysts are substances which use absorbed light to produce photoexcited electrons. These photoexcited electrons are then transferred from the valence band gap to the conduction band gap [15]. This process generates electron–hole pairs (e−/h+) which act to reduce and/or oxidize organic compounds and decompose water adjacent to the catalyst surfaces [16–19]. Heterogenous metal oxides such as TiO_2, ZnO, SnO_2, and CeO_2, are naturally occurring, abundant, and widely used in photocatalytic applications because of their ability to produce positive electrons holes. While various heterogeneous photocatalysts have been studied and utilized [20–23], titanium dioxide has received the most attention for organic contaminant degradation [24–26]. Titanium dioxide possesses photostability and low toxicity, making it a superior catalyst for organic pollutants [27–29].

Sol-gels form during a chemical reaction, hydrolysis/condensation, between a precursor and water, which promotes a biphasic cross-linking of silica-oxygen bonds to create a stable gel structure. Silica solutions formed during cross-linking of chains convert monomers into a colloidal media that can be further evolved into discrete particles or networked gel semi-solids. Two major families of sol gels exist, xerogels and aerogels which are differentiated based upon the method for extraction of solvent solutions from the network of cross-linked gels. Within both aerogel and xerogel processes, metal oxides are utilized as dispersant aids and as additives to the final gel structure. In particular titanium is used for multiple purposes, but the xerogel sol gel process is widely utilized as a method for producing doped and uniform photocatalysts.

Sol-gel processes are an innovative methodology for developing nanoparticles used for treating emerging contaminants of concern, especially when addressing organics. The sol-gel synthesis process allows for the usage of the anatase phase of titanium dioxide, which has a

larger band gap (3.2 eV) than rutile (3.0 eV). A larger band gap has been shown to reduce the light absorbed but increased the oxidation ability of electrons [30]. The photocatalytic capabilities of titanium dioxide can be further enhanced by doping the nanoparticles with various other transition metals such as iron, niobium, and chromium [31]. However, leaching of the doped species often occurs and is cause for concern if dopants are toxic metals such as chromium [32].

One major advantage of incorporating photocatalytic materials within the sol-gel process is the ability to promote an increased surface area of the photocatalyst during gelation. Optimization or homogenization of the combined materials occurs as the catalyst disperses evenly throughout the gel, creating a uniform surface area, particle size, and distribution. In turn, increasing surface area enhances the efficiency and effectiveness of catalysis because of the homogenous structure created [33,34]. Recent advancements in sol-gel synthesis processes indicate that controlling the molar ratio of water-to-surfactant may increase the BET surface area by up to 58% [35]. Sol-gel synthesis is cost-effective, requires low energy consumption, and has the potential to produce zero waste during production [36]. When considering synthesizing photocatalysts for water and wastewater treatment, the xerogel method is most commonly used to develop catalysts to obtain nanoparticles for use in part with slurry reactors [37]. While using a slurry method optimizes the surface area of reactive sites available during treatment, the systems require a secondary or membrane filtration to retrieve the photocatalyst and ensure nanoparticles are not introduced to the environment as contaminants [38]. Others have developed silica-based adsorbents designed to filter out organic contaminants at high concentrations [39,40].

Research herein describes an innovative, photocatalytic sol-gel matrix technology that creates a stabilized porous granular media through the utilization of sodium hydroxide, a known foaming agent [41], during solvent extraction. Sodium hydroxide pore infiltration followed by subsequent foaming during firing, aids in retention of the sol-gel networked structure. The resultant material is a very light-weight, highly porous, photocatalytic granular media which can be used as a packed-bed or column treatment systems. Granular media provides for a continuous treatment of contaminated solutions without requiring secondary filtration to recapture the activate treatment agent or photocatalyst. In addition, the porous, absorbent structure of this media creates micro and meso pore spaces that can be leveraged to further treat solution using an electrophilic or nucleophilic attack without need for separate injection. When both photocatalytic and electrophilic or nucleophilic means for treatment are combined, dual treatment can be passively accomplished by engineering the pore structure and diffusive rate of the electrophile or nucleophile. Further, this pore space can be utilized to passively diffuse buffer solutions for waste streams which require specific pH ranges for optimal treatment to occur. The research presented below demonstrates the reproducibility of the granular structured media, validates the destructive capabilities of the media with bench scale photoreactors, and further defines the long-term sustainability of the media during continuous treatment.

Results and Discussion

Four concentrations of silicic acid underwent experimentation in order to determine process optimization, SGM product durability, and photocatalytic capabilities (Figure 1). Process characterization and discrete particle testing were performed using thermal gravimetric analysis, forensic inspection using scanning electron microscopy and mercury intrusion

porosimetry. The results of particle and/or process characterization are separated below from the corresponding photocatalytic capabilities as the physical engineered characteristics dictate the photocatalytic nature of the SGM.

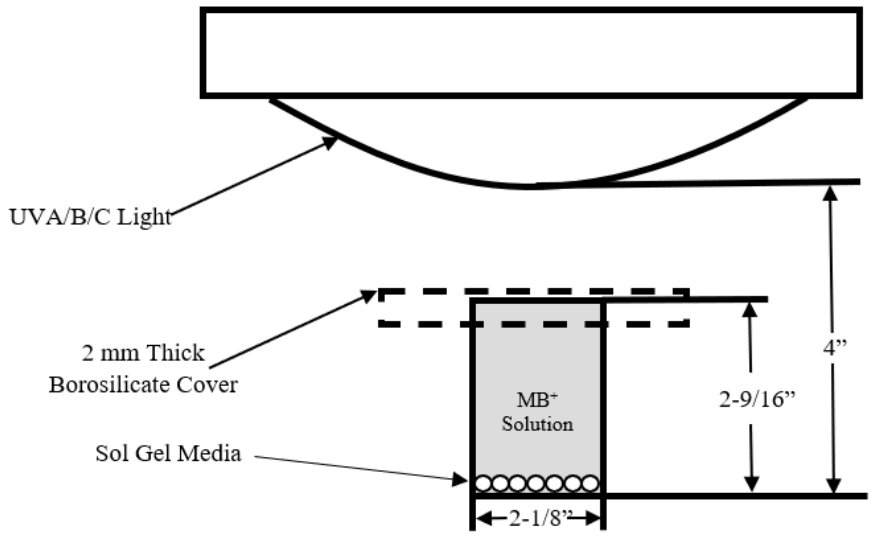

Figure 17 – Photocatalytic Testing Setup Adapted from ISO 10678.

Photocatalytic Porous Silica-Based Granular Media Characterization

In order to determine the thermal stability of the SGM before and after firing, as well as to measure the mass fraction of volatile components present in the pre and post fired SGM, thermal gravimetric analysis (TGA) was performed. TGA was used to evaluate both the SGM during the gel phase, after being soaked in NaOH, and after complete synthesis of the SGM, post firing. Figure 2 depicts the thermal stability of the SGM as the mass evaluated underwent the firing process described above as compared to the gel phase. A 52% mass loss was recorded during the SGM firing process which directly corresponds to the evaporation of the solvent, or liquid phase, at increasing temperatures. When the gel media is compared to the fired SGM

using TGA, very little mass loss is observed, approximately 2%. Minimal mass loss indicates that the pore volume is retained by the foaming agent introduction, supporting the hypothesis that the sodium hydroxide effectively replaces the solvent after 12 h. Additionally, TGA analysis reveals that SGM is stable after firing over a range of temperatures and therefore capable of performing treatment over this range. SGM voids that formed during the gelation process are very clearly demonstrated to be preserved due to the foaming agent, yet the pore volume, structure, and distribution cannot be evaluated using TGA. If these pore structures are to be utilized as a means for additional treatment agents such as a nucleophile or electrophile, characteristics of the pore space distribution, volume, and gradation with respect to the variables of firing temperature and silicic concentration must be evaluated.

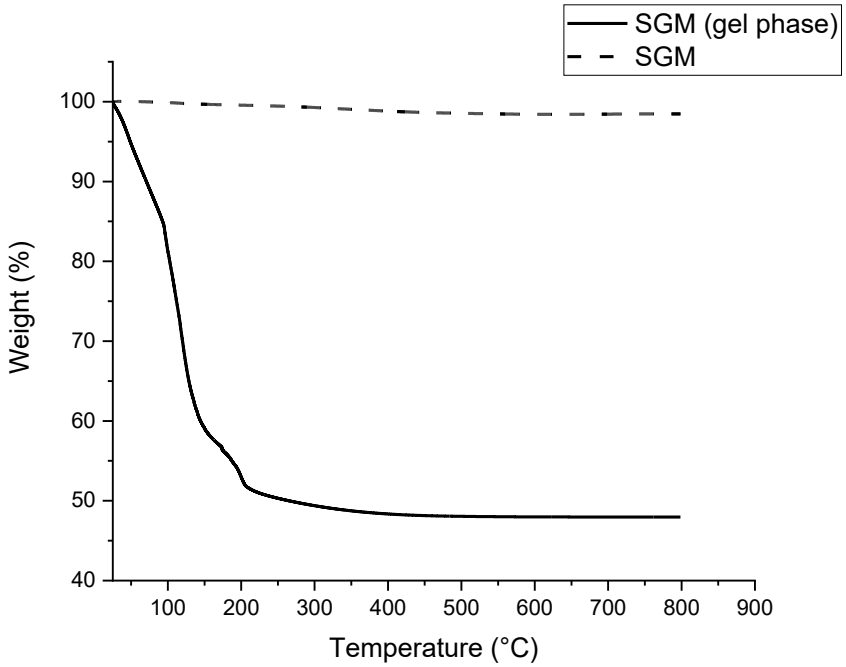

Figure 18 – Thermal Gravimetric Analysis on Percent Weight loss of SGM during firing.

In order to evaluate the effects of the variables of increasing firing temperature and silica concentrations, visual verification of the pore space post firing was needed. Representative SGM samples randomly selected from each batch were preserved, broken to expose the internal pore space and then prepared for SEM analysis by mounting the samples onto carbon tape. Each sample was examined for pore space using a width of field view from 10 to 12 mm (noted as WD in Figure 3) in backscatter mode and then further evaluated for elemental composition using the electron dispersive spectroscopy (EDS) function. Figure 3 depicts the cross-sectional view of the sample SGM pieces as silicic acid concentrations increased from 5, 50, 500, to 1000 mg/L. Upon visual inspection two distinct forms of void structures are present within the distribution across the cross section. Large void spaces formed during the rapid evaporation and activation of the foaming agent during firing are more readily observed in the SGM containing lower concentrations of silicon. Foaming agent induced pores decrease in abundance and relative size as function of increasing silica in the SGM. This decrease in degassing related pores indicates that the cross-linked polymers are stronger and more durable as silica content increases. There is a background distribution of micro to meso scale pore spaces formed during the cross-linking of the polymer structure. Polymer cross-linked structure preservation, uniformity, and homogenous size distribution all appear to be directly correlated to increasing silica content within the SGM (the void in the bottom left corner of Figure 3D is a hole in the SGM and is not representative of the SGM structure). An important yet more subtle feature which also corresponds to increasing silica content is the increase in the tortuosity and permeability of the pore space. While the cross-link formed pore-spaces appear smaller in average size, they also appear more interconnected, homogenous in distribution, and uniform in size. An increase in cross-linked structures and decrease in

degassing voids can be observed as silicic acid concentrations increase. The increase in cross-linked structures is caused by the increase in nucleation sites the silicic acid brings, thus creating a more durable SGM. Increases in durability and strength of the SGM are demonstrated to improve as the degassing void space decreases and silicic acid concentrations during gelation increase. While structural and thermal strengths have been assessed, the purpose of the SGM is to function as a photocatalytic granular media for water treatment.

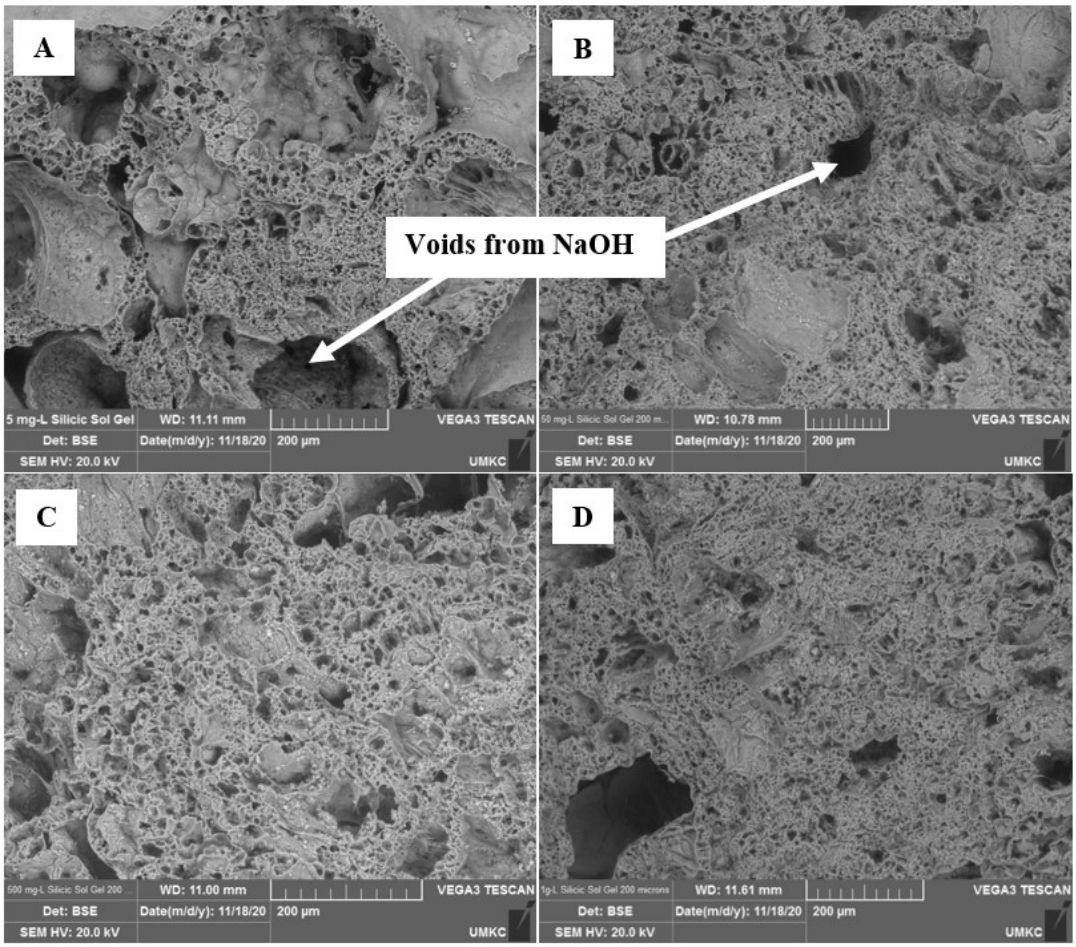

Figure 19 – SEM Images of (A) 5 mg/L Silicic Acid SGM (B) 50 mg/L Silicic Acid SGM (C) 500 mg/L Silicic Acid and (D) 1000 mg/L Silicic Acid.

A diffusion pore space capable of storing an absorbed solution is observed in the cross-section of SGMs in Figure 3. In order to determine the capacity of the SGM, absorption testing was performed on the various SGM in accordance with ASTM C128 [42]. The test was modified to have an extended saturation period of 72 h due to the presence of significantly more void space relative to traditional aggregates. No other deviations from the standard occurred. The percent absorption was found to be between 50% and 65%, depending on the variation. It is important to note that absorption was observed to decrease with the increase of silicic acid which corresponds to the larger voids formed during off-gassing of foaming agents. Desorption or diffusion of solution from the pore space is dictated by the formation of a thin crust that formed during the firing process. One way to measure the crust thickness or internal to external interface is through mercury intrusion porosimetry (MIP) which evaluates porosity, pore size distribution, and pore volume by intruding mercury into pore space under pressure. At low pressure, the large pore spaces are filled. As pressure increases, mercury is forced into the smaller pores. This process is governed by the Washburn equation which describes the pore aperture as a function of pressure using the non-wetting liquid physical properties. Table 1 presents the results of the MIP analysis performed on four samples representing increasing silica contents.

Table 3. Pore Distribution Characteristics and Properties.

	5 mg/L	**50 mg/L**	**500 mg/L**	**1000 mg/L**
Intrusion Data Summary				
Total Intrusion Volume (mL/g)	0.9984	0.8768	1.2206	1.0791
Total Pore Area (m/g)	33.152	34.260	34.450	38.723

Median Pore Diameter (Volume, nm)	750.9	1162.6	1249.6	1014.0
Median Pore Diameter (Area, nm^2)	17.4	14.9	16.3	16.0
Average Pore Diameter (4V/A, nm)	120.5	102.4	141.7	111.5
Bulk Density at 0.20 psia (g/mL)	0.5349	0.5981	0.4767	0.4998
Apparent (skeletal) Density (g/mL)	1.1478	1.2576	1.1399	1.0849
Porosity (%)	53.4006	52.4428	58.1829	53.9323
Stem Volume Used (%)	57	46	61	59
Pore Structure Summary				
BET Surface Area (m^2/g)	162.3000	133.9600	129.2300	156.9500
Tortuosity factor	0.032	0.065	0.044	0.032
Tortuosity	0.9166	1.3234	1.1439	1.2185
Mayer Stowe Summary				
Interstitial porosity (%)	35.0388	36.3433	28.8441	25.9500

It is clear from the MIP pore structure analysis that increasing amounts of silica up to 500 mg/L created a more uniform pore structure, overall porosity, and average pore diameter and volume. Increasing silica higher, to 1000 mg/L, did not produce a more desirable pore structure or overall porosity. Within the 500 mg/L silica SGM, a well graded distribution of pore space is noted, as the average and median pore diameter and volume are both greater than any other variation. BET surface area is a measure of catalyst surface area available to react with a gas or solution. BET surface areas are approximately 33–40% higher than rare titanium dioxide surface area. In addition to pore structure and characterization, the distribution of the pores was compared to differential pressure of intrusion agent. Pore size distribution is

calculated with the assumption that the pores are spherical and that larger pore spaces fill with the non-wetting liquid intrusive agent at lower differential pressures, and smaller pores require significantly higher pressure to fill. The distribution curve of pores for the 500 mg/L SGM is presented in Figure 4. Pore distribution is bimodal in that there are large pore spaces that are homogenous in shape and size, while the majority of pore spaces are much smaller with an average size of 80 nm. The bimodal distribution also indicates that there is a 30–40 nm thickness of very dense layer surrounding the smaller pores which is noted in Figure 4 as the curve transitions from horizontal to vertical. All four SGM concentrations examined depicted the same bimodal distribution with the same pore size distribution transition. A working hypothesis is that the crust or shell layer separating the larger pores from the smaller pores is formed as the foaming agent degasses during firing. The exterior of all SGM variations is smooth with no obvious openings, providing some validation of this theory. In addition, the absorption and desorption of solution from the pore space indicates a bimodal trend with larger pores sorbing and desorbing solution faster than smaller pores. The rate at which desorption occurs mimics the pore distribution curve in Figure 4, both of which describe a thin film behavior. The thin shell may function as a control on diffusion of solution from within the microporous structure to solution surrounding the exterior of the media.

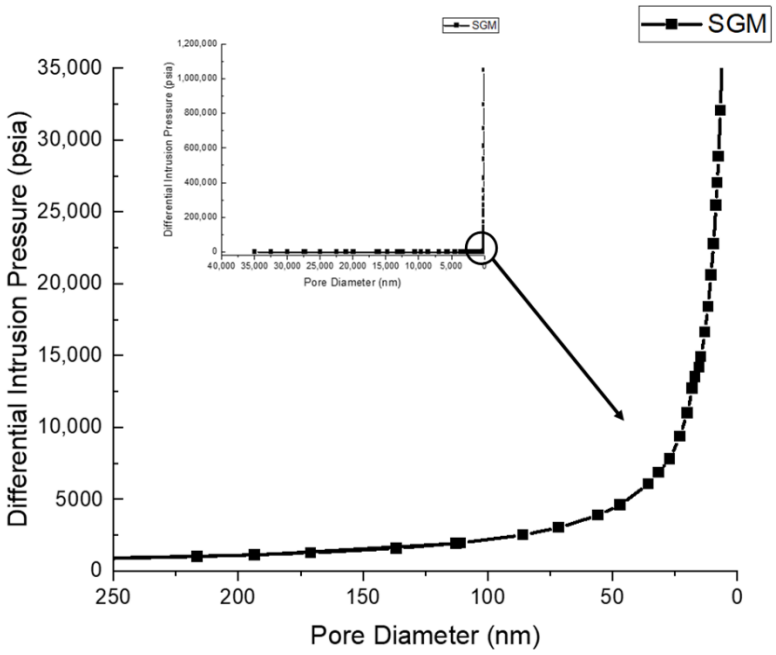

Figure 20 – Mercury intrusion porosimetery pore size distribution.

Since the SGM was developed as a granular photocatalytic material, understanding the amount and phase of semi-conductor metal used in the media is extremely important. In order to evaluate the source and final photocatalysts, powdered x-ray diffraction (XRD) was performed to determine the major composition of the source. XRD analysis revealed that calcination of the semiconductor metals may have occurred during the firing stage. While both anatase and rutile phases are still present, the intensity of the rutile peaks significantly decreased after the SGM synthesis media process.

Photocatalytic Degradation of Methylene Blue

Degradation Kinetics

Photocatalytic reactivity testing was performed on all four variations of SGM utilizing the ISO methodology described in 3.1 (Figure 1). SGM was adhered to the batch reactor to prevent flotation and to ensure that each reactor maintained the same exposed surface area.

SGM granules were prewetted to saturated surface dry condition prior to testing. Sample aliquots for each silica concentration SGM were taken every ten minutes from 0 to 60 minutes as shown in Figure 5. A control was run with no light to validate the degradation of the dye versus adsorption to the SGM. Figure 4 depicts some minimal observed adsorption occurs from 0 to 30 minutes as the dye wets the surface and the pore space fills, however, there is no change from 30 to 60 minutes. The primary mechanism for methylene blue reductions by SGM is therefore photolysis, when the dark control data is compared to the data presented in Figure 5. While similar degradation percentages were obtained from all treated SGM variations at 60 minutes, the 500 mg/L silicic acid SGM had the quickest path to degradation and resulted in 90.6% removal, while the majority of removal (84.6%) removal was achieved after 40 minutes. The rate of reduction clearly slows down in all reactors as time approaches the hour mark.

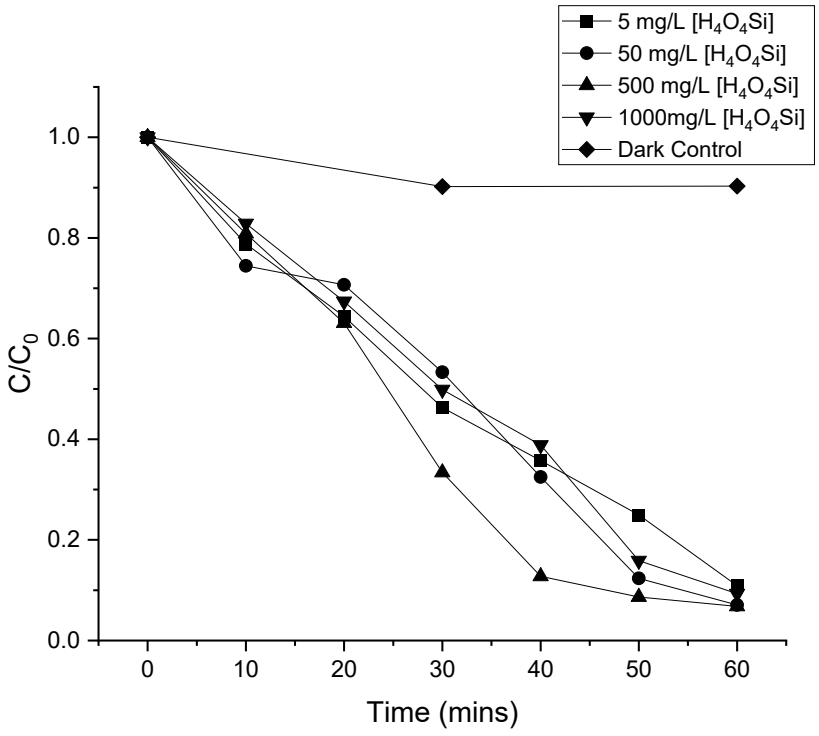

Figure 21 – Percent Photocatalytic Degradation of Methylene Blue Over Various SGM.

Photocatalytic degradation of methylene blue in SGM is shown to follow first-order degradation kinetics (Figure 5). Figure 6 depicts the linear trend when timed discrete aliquots are plotted against $\ln(C_0/C)$. The variance from the fitted line is theorized to be from minimal evaporation of the dye during treatment causing some concentration or from pH influence, as discussed later. Table 2 gives the regression equations and rate constants for the various SGM where the r-squared value is approaching 1 indicating a first-order reaction.

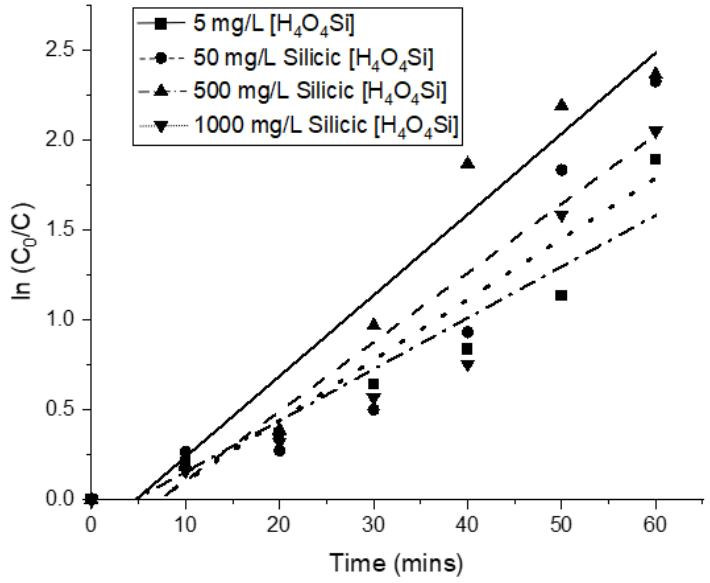

Figure 22 – Reaction Kinetics of Methylene Blue Over Various SGM

Table 4. Regression Equations and Apparent First-Order Rate Constants for Degradation Kinetics of Methylene Blue Over Various SGM.

Silicic Concentration of SGM (mg/L)	**$\ln(C_0/C) = kt + b$**	**R^2**	**k (min^{-1})**
5	$\ln(C_0/C) = 0.0286t - 0.131$	0.924	0.0286
50	$\ln(C_0/C) = 0.0385t - 0.278$	0.8882	0.0385
500	$\ln(C_0/C) = 0.045t - 0.2114$	0.9522	0.045
1000	$\ln(C_0/C) = 0.0337t - 0.2342$	0.9054	0.0337

Effect of pH on Degradation Kinetics

Literature states the initial pH of MB^+ is between 5.0 and 8.0 S/U, when water is used as a solvent [43]. For this study, the initial MB^+ pH was 6.55. The pH was measured with an Accumet gel-filled electrode calibrated with a standard pH 4.0, 7.0, and 10.0 curve. Measurements of pH occurred over various time increments, in 10 minutes intervals for the entire hour of photostimulated treatment. Figure 7 shows an increase in pH over time and with degradation of MB^+. This trend opposes general photocatalyzed reactions, considering the byproducts of MB^+ destruction are acidic compounds [43]. The increase in pH is assumed to be diffused excess sodium hydroxide from within the SGM. In order to support this hypothesis, diffusion testing was performed using a 10 to 1 ratio of DI water to SGM. The test was performed on the 500 mg/L silicic acid SGM considering it was the most reactive and all variations followed a similar trend. Figure 8 shows that the pH of a solution increases during continuous contact time with the SGM until equilibrium is reached at about one hour. The extent of this influence is unknown considering no change to the ending pH was observed during cycle testing. Methylene blue degradation is shown to increase with basicity; therefore, the degradations kinetics could be impacted by the increase in pH.

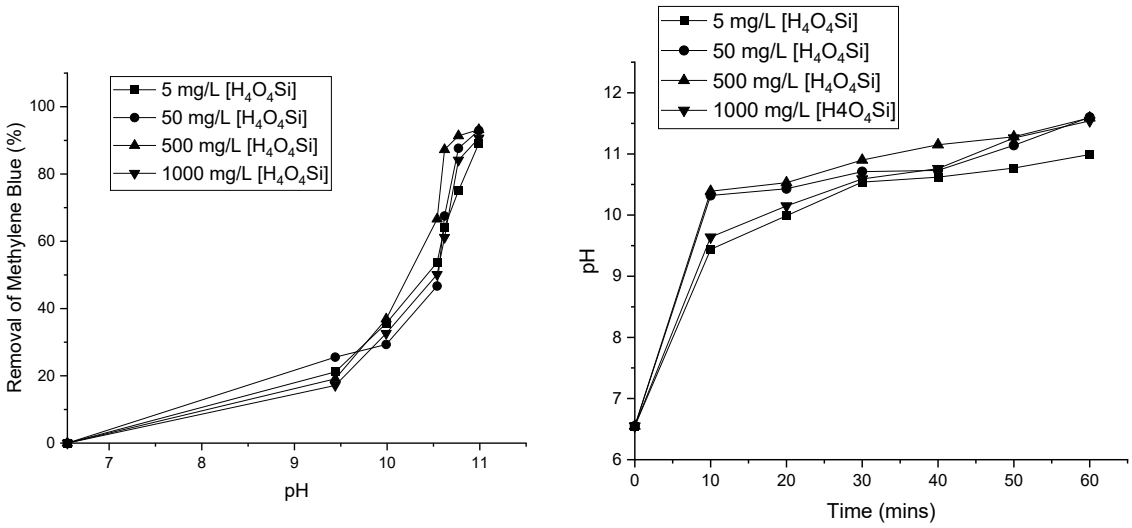

Figure 23 – pH of Methylene Blue Over Various SGM

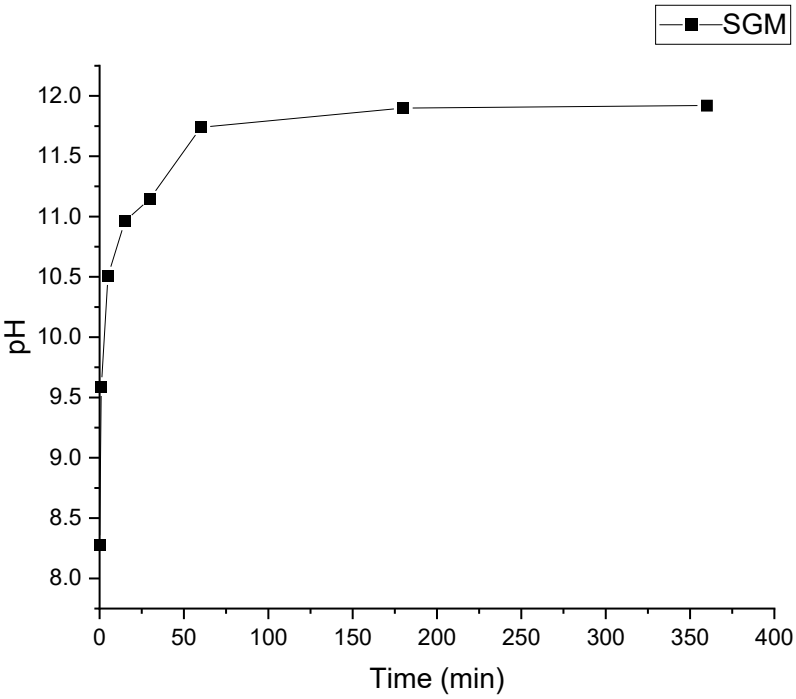

Figure 24 – SGM Influence on pH.

While full wavelength spectra analysis was performed on every sample. The 500 mg/L silicic acid SGM is depicted in Figure 9 because it was proven to be the most reactive. Here it can be more easily observed that the degradation percentage is the greatest between 20 and 30 min. Similarly, the greatest increase in pH was found to be from 20 to 30 minutes, further validating the influence of pH on degradation kinetics.

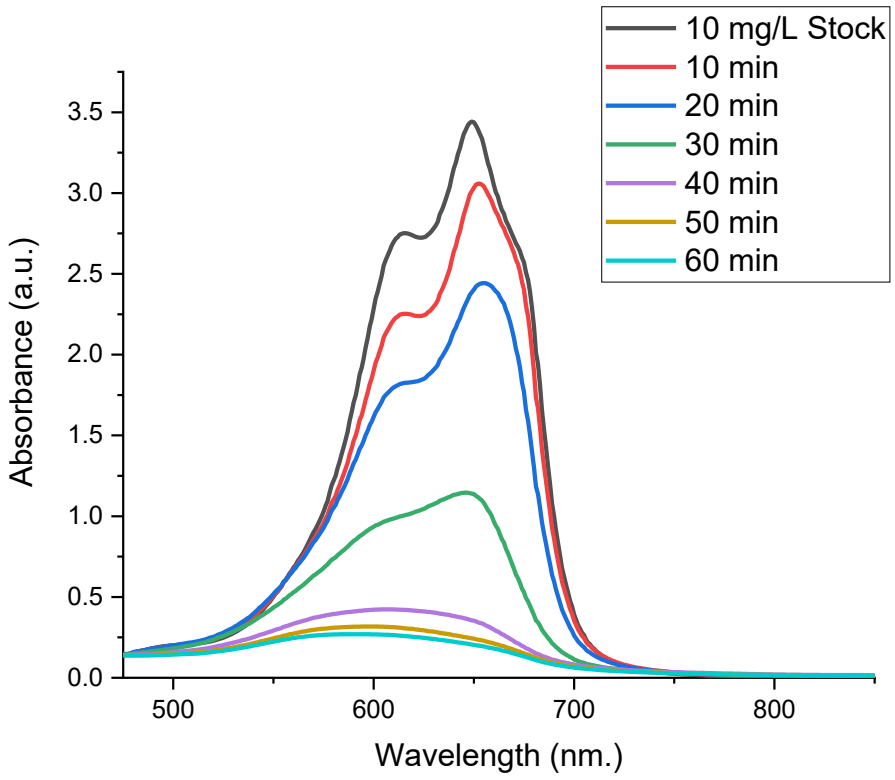

Figure 25 – Methylene Blue Degradation by 500 mg/L Silica SGM

Sustained Photocatalytic Reactivity with Added Amendments to the SGM

The variations of SGM were further tested in a cyclic form with additions of de-ionized water (H_2O-SGM), nitric acid (HNO_3-SGM), and sodium thiosulfate ($Na_2S_2O_3$-SGM) to the pore space. SGM media were adhered to the reactor, filled with MB^+ solution, tested, the

solution decanted from the reactor, and then refilled for another reactor test cycle. SGM without anything loaded in the pore space was tested as a control for comparison of performance. For this study, the amendments were preloaded into the pore space by soaking the SGM in a one molar concentration of their respective solutions for 72 h. Vacuum impregnation could be used as an alternative to soaking to ensure that all pores are preloaded with the diffusive solution of choice. Cycles were performed in 45-minute allotments and recycled a total of four times (Figure 10).

The stability and reactivity of the SGM were analyzed by the removal of MB^+ and the visual appearance of the media over each cycle. For cycle 1, the unsoaked granule noted in Figure 10 as "SGM" was found to decrease in MB^+ treatment removal as the content of silicic acid concentrations increased (Figure 10 a–d). Increasing silica appears to inhibit the ability for the dye to absorb onto the surface of the photocatalyst as increasing silica within the SGM encapsulates the titanium dioxide. Considering the short lifespan of reactive radicals, they are normally diffused to the photocatalytic surface and react with the adsorbed molecules. Therefore, the longer it takes for the contaminant to adsorb to the surface, the longer it will take to remove the compound. This phenomenon is only observed in cycle 1 of all "SGM" labelled batches across all four concentrations, as the surface and pore space were wetted in subsequent cycles the performance was comparable to the other treatments.

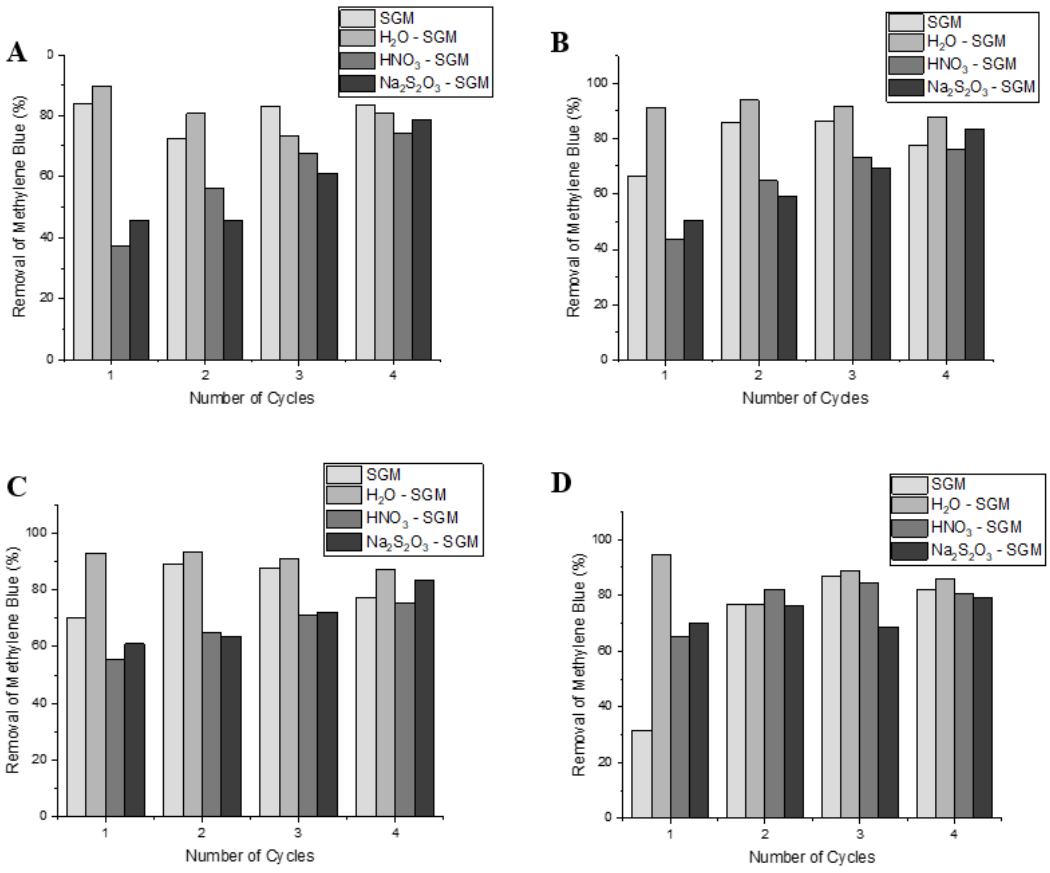

Figure 26 – Photocatalytic Cyclic Testing over (A) 5 mg/L Silicic Acid SGM (B) 50 mg/L Silicic Acid SGM (C) 500 mg/L Silicic Acid and (D) 1000 mg/L Silicic Acid, with various amendments.

The addition of both nitric acid and sodium thiosulfate treatments hindered the removal efficiency for MB^+ for all concentrations but is most pronounced in the SGM batches corresponding to higher absorption capacities (5 and 50 mg/L silicic acid). However, the addition of nitric acid has the ability to act as an internal pH buffer in acidic conditions (Figure 11). Future uses of the internal pore space could include various treatments which diffuse from the microstructure of internal pores, through the thin shell of the SGM, and then contribute to the overall wetting solution. In these situations, the desired acid and concentration to preload

into the SGM would be determined by the compounds of concern in the waste stream and optimal final pH for degradation. Cyclic testing verified the ability of the SGM to buffer the solution to a pH equivalent to the equilibrium of the media, which was determined to be just under pH 12.0 during diffusion testing. The stability and durability of the SGM becomes a concern when the pH of solution exceeds the natural pH of the media. Of primary concern is cleaving of silica–oxygen–silica bonds at pH elevated above 12.0. Therefore, no addition treatment agents can be incorporated within the pore space that will increase the pH greater than 12 for a sustained amount of time. The pH of the SGM with no additional treatments and DI water addition were statistically indifferent, therefore, only one was reported. The sodium thiosulfate incorporated within the pore space had no influence on the pH.

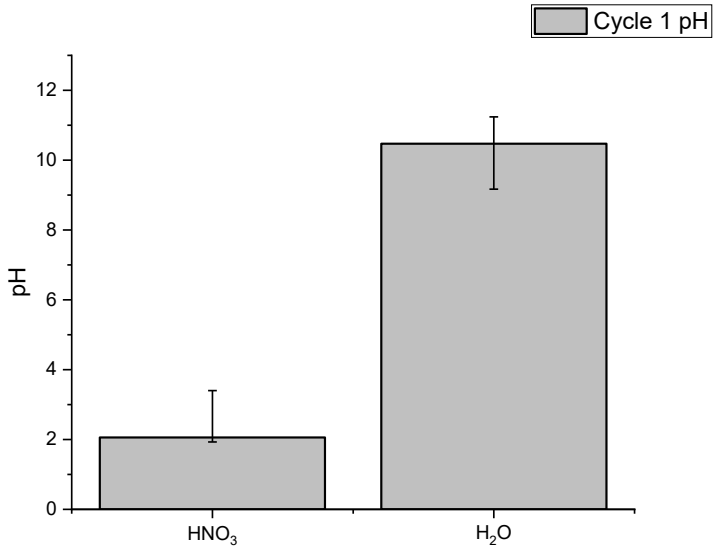

Figure 27 – pH of Methylene Blue After One Cycle.

The longevity of the SGM was tested over four continuous cycles. General trends showed the DI water soaked SGM consistently performed better at all variations of the media. While there was some variance in the removal of MB^+ over cycles, the percent removed stayed

between +/−10%. The 50 mg/L and 500 mg/L were the most consistent SGMs, with removal only varying between +/−5%. Further testing was performed on these SGM variations to determine the optimal mixture design for the removal of methylene blue.

Determination of the Most Efficient SGM

Cyclic testing was performed for six cycles over both the 50 mg/L and 500 mg/L SGM to determine which SGM was most effective in the continuous removal of MB^+. The SGM was soaked in DI water for 24 h prior to testing and then dried to saturated surface dry condition. The SGM was tested utilizing both 10 mg/L and 20 mg/L methylene blue to test the reactivity at higher contaminant concentrations (Figure 12). Cycles were performed in 60-minute allotments and continuously recycled.

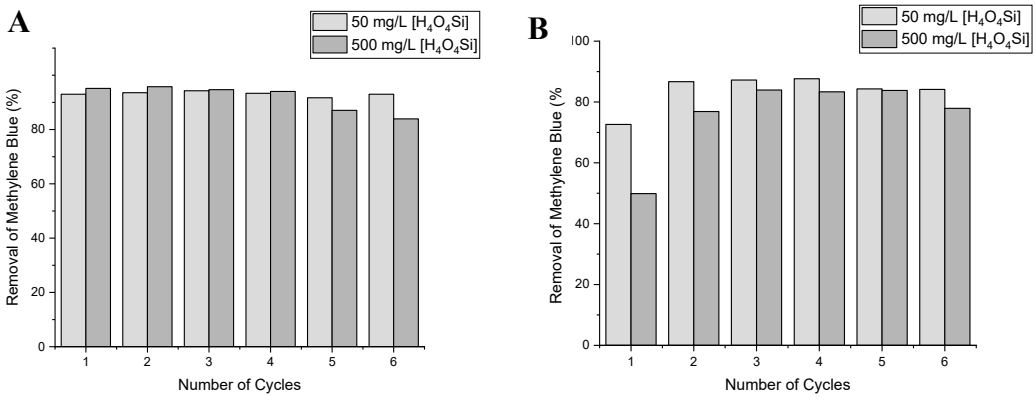

Figure 28 – (A) 10 mg/L Methylene Blue Degradation by SGM (B) 20 mg/L Methylene Blue Degradation by SGM.

Advantages and disadvantages of both SGM variations were observed during cyclic testing. For the 10 mg/L MB^+, maximum removal was 94.29% for the 50 mg/L silicic acid SGM (50-SGM) and 95.79% for the 500 mg/L silicic acid SGM (500-SGM). While the 50-SGM varied less than 2% over cycles with continuous removal over 90%, the 500-SGM varied

just over 10%. The 20 mg/L MB^+ had a maximum removal of 87.65% for the 50-SGM and 83.83% for the 500-SGM. The first cycle had a significantly lower removal percentage which is assumed to be a delay in the adsorption of the dye to the photocatalyst to begin degradation.

While the absorbance of MB^+ over cycles was used to determine efficiency of the SGM, visual observations were also made. Solids appeared in the solution of the 50-SGM in the 4th cycle but did not seem to have a large influence on the absorbance of the MB^+. No solids were visible in the 500-SGM. This observation notes that the stability of the structure of the SGM increases with silicic acid concentration.

The photocatalytic reactivity of both the 50-SGM and 500-SGM show continuous removal capacity of methylene blue. The 50-SGM shows a higher efficiency of removal in both concentrations of MB^+ by the sixth cycle. However, the durability and stability of the 50-SGM significantly lessens overtime, therefore, the 500-SGM is determined to be the most suitable SGM for continuous treatment of methylene blue.

SGM Condition after Cyclic Testing

After cyclic testing was completed, forensic analysis was carried out on the SGM to determine the condition of the photocatalyst. Figure 13 shows the distribution of the silicon and titanium within the SGM in SEM-EDS at microscale. In the image areas colored red are titanium, while those colored blue are silicon. In SEM-EDS imagery the darker and more intense the color, the higher the concentration of that element. While there are some places with either one of the elements is more predominant, it can be observed that the photocatalyst is homogeneously immobilized within the media and does not appear to leach out over time. Fixating the photocatalyst within the SGM is one priority factor that allows SGM to

continuously perform treatment without the need for secondary filtration unlike slurry treatment technics.

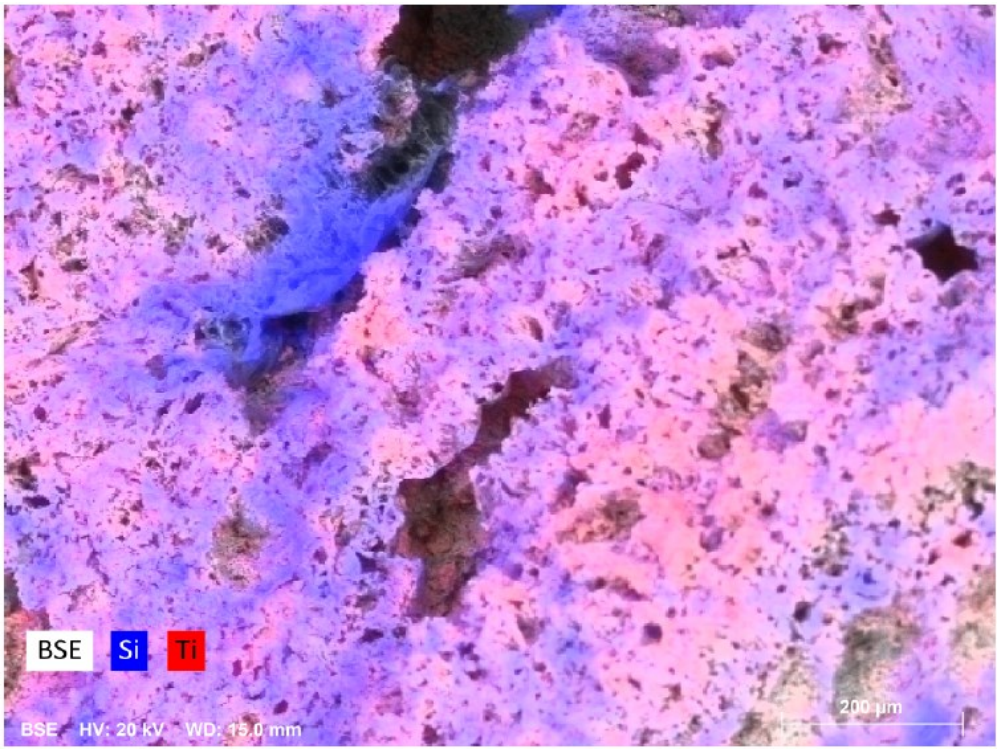

Figure 29 – SEM/EDS Image of SGM after Cyclic Testing.

While fixation of the photocatalyst is an important aspect of SGM, it is still possible for a fixated photocatalyst to convert to other forms or the ratio of anatase to rutile may change. XRD analysis was performed on the SGM before and after cycle testing (Figure 14). The titanium dioxide (P25) used in synthesis of the SGM was analyzed for comparison of the anatase and rutile peaks. While the intensities of the peaks were suppressed by the silica content in the SGM, it is apparent that the peaks do not shift or broaden in the anatase and rutile peaks noted. Also, no notable changes were exhibited in the SGM patterns before and after cyclic testing, showing no alterations to the SGM occur during testing.

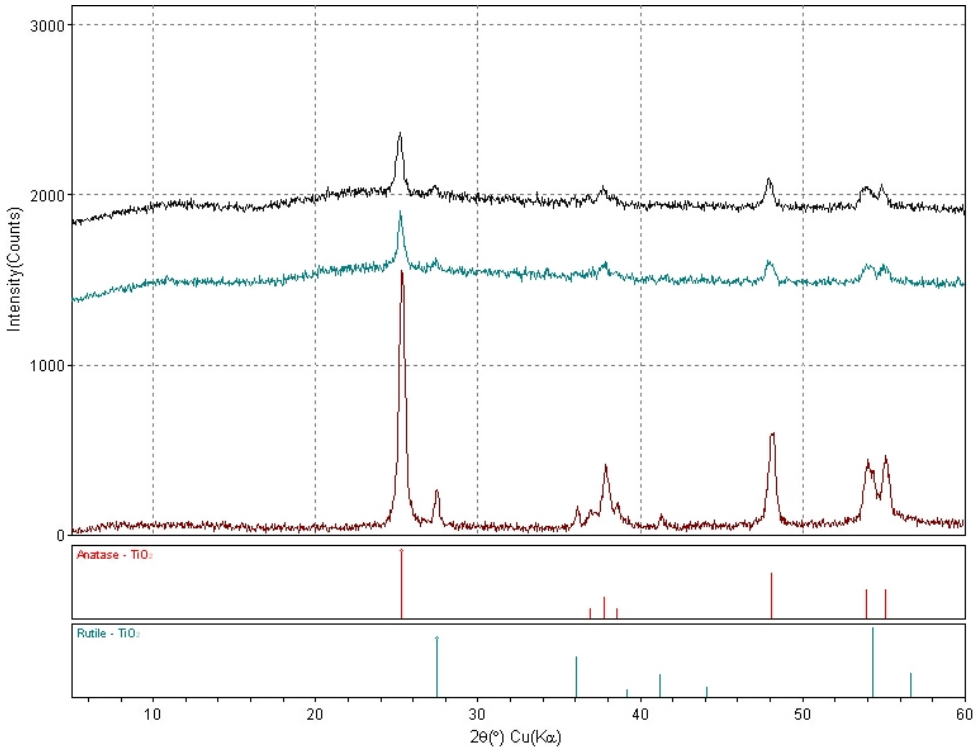

Figure 30 – XRD Pattern of SGM Before and After Cyclic Testing Compared to the TiO_2 Photocatalyst Used.

Experimental Methods and Materials

Materials

Materials utilized to create the stabilized sol-gel structure and used in photocatalytic testing include the alkoxide precursors, acid and base catalysts, photocatalysts, foaming agents, electrophiles, and nucleophiles. Tetraethyl orthosilicate (TEOS), tetramethyl orthosilicate (TMOS), titanium (IV) oxide, Aeroxide ® P25, ACROS Organics, and nitric acid were purchased from Thermo Fisher Scientific (Waltham, MA, USA) with lot numbers A0420038, A0408640, A0407014, and 147594, respectfully. Sodium hydroxide (B1750262), potassium hydroxide (B1558512), and silicic acid (B0148079) were purchased from Sigma Aldrich (St. Louis, MO, USA). Reagent grade sodium thiosulfate, acetic acid, and hydrochloric acid were

used. In order to determine the long-term sustainability of the media over time, initial X-ray diffraction (XRD) analysis of the titanium dioxide (TiO_2) was performed and yielded a composition primarily composed of anatase with minor rutile.

Photocatalytic Porous Silica-based Granular Media Development

The overarching goal of this research was to develop a porous, photocatalytic, granular media to be utilized in a packed column or bed, for passive, continuous treatment of organic contaminants in solution. Optimal combinations of precursor to water mixtures were performed in bench scale testing using an iterative, partial factorial approach that controlled for concentration, ratio, and process. In order to determine the most favorable conditions and processes, photocatalytic porous silica-based media (SGM) synthesis was conducted with various precursors, acid catalysts, base catalysts, material ratios, temperature, and solvent extraction processes to determine a suitable media for continuous treatment of methylene blue.

While both tetraethyl orthosilicate and tetramethyl orthosilicate were examined as viable precursors for structural stability of SGM, TEOS is the more cost effective and industrializable precursor for SGM applications. The addition of acid and base catalysts was used to control the time to gelation and ultimate a porous structure. Acetic acid, hydrochloric acid, silicic acid, nitric acid, sodium hydroxide, and potassium hydroxide were examined in a testing matrix of concentration and volume over various TEOS to water ratios. While all of the examined acids and bases listed were suitable for developing a sol-gel, strong acid and bases heavily favored the irreversible forward reaction hence creating a very weak cross-linked structure. Silicic acid the most appropriate catalyst as silica acts as a nucleation site during polymerization as well as possessing the ability to lower the solution pH sufficiently to

promote hydrolysis without introducing leachable compounds to the SGM. In addition, since silicic acid is a weak acid, gelation was readily controllable during heating.

Aerogels are ultralight, porous materials in which collapse of the gel network is prevented by replacement of solvent by gas. Solvent extraction to develop a porous media include supercritical drying, ambient pressure with matrix strengthening, or freeze-drying methods, leading to the synthesis of an aerogel [44,45]. Of these three methods, supercritical drying is the most commonly utilized variation of aerogel solvent extraction. Supercritical drying requires special pressure vessel capable of high pressure, in which supercritical carbon dioxide is continuously passed over the gel to extract the solvent. Super critical drying requires specialized equipment, skilled technicians, and potentially harmful gas to reproducibly synthesize aerogels. With the introduction of a foaming agent into the solvent system, described below, supercritical conditions were bypassed as unnecessary. While various foaming agents or hydroxides were tested for maximum pore structure retention with minimum loss of material, sodium hydroxide yielded the best results. Sodium hydroxide was introduced to the sol-gel in gelation phase prior to firing at various concentrations in order to determine optimized conditions. This step proved to be crucial to the sol gel media process as higher concentrations of NaOH cleave the Si–O–Si bonds that make up the gel network [46] and result in the dissolution of the gel. However, too low of a sodium hydroxide concentration over short lengths of exposure did not fully allow for foaming agent penetration, resulting in the gel forming powder upon firing. Once optimal concentrations and immersion times were determined for sodium hydroxide, the media was placed on a ceramic sheet and fired. Various activation temperatures were utilized in order to optimize the foaming agent's release from the pore solutions and therefore produce the most homogenous and well distributed pore structure.

Note that the foaming agent is not activated at ambient conditions and requires some heat to retain the 3D cross-linked network. A temperature over 300 °C was required for activation of the foaming agent, however, above 450 °C the titanium photocatalyst converted to predominantly rutile.

Once the general process for SGM was devised, further testing for the optimal mixture proportions was performed. Initial SGM synthesis and photocatalytic testing indicated the optimal silica to titania ratio for structural stability and reactivity was approximately a 4:1 (SiO_2:TiO_2) ratio. Addition of titanium dioxide exceeding this ratio produced a powder upon firing, rather than a porous media. Silica in excess of the 4:1 ratio inhibited or shielded the photocatalyst within the media or on the surface, causing the media to be less photocatalytically active. Trends showed durability of the SGM structure increased with an increasing concentration of silicic acid up to an optimized point before reactivity began to decrease due to armoring of photocatalyst discussed above. This study further investigates the extents of this trend to determine the optimal SGM mixture for continuous cyclic batch testing of the photocatalytic removal of methylene blue.

Photocatalytic Porous Silica-based Granular Media Synthesis

Media synthesis was performed following a hydrolysis/condensation reaction mechanism [47] and utilizing TEOS as a precursor, silicic acid as a catalyst, and TiO_2 as a photocatalyst. During this process, 9 g of TiO_2 was dissolved in 150 ml of TEOS and 150 ml of silicic acid at various concentrations (5, 50, 500, and 1000 mg/L). The solution was stirred at 55 °C until gelation was complete, approximately 12 h after initial mixing. The gelled sample was then broken into the desired size or gradation for the testing protocol needed, e.g. column or batch reactors. For this study spherical pieces about 1 cm in diameter were created in order

to match the reactor vessel. Pieces of the broken gel were placed into 1M NaOH for a minimum of 12 h to allow for the foaming agent to displace solvent within pore space. However, with the chosen concentration, less than 2% of the gel mass was lost during the soaking process. Once the gel was fully saturated with the foaming agent (NaOH), the gel was fired at 400 °C. Four variations of SGM at increasing concentrations of silica were chosen for further analysis and photocatalytic efficiency testing. In addition, forensic investigation of the structure and durability of the SGM was performed using scanning electron microscopy (SEM) (UMKC) imagining and mercury intrusion porosimetry (MIP) (Tuscon, AZ, USA) to analyze the porosity and pore distribution.

Photocatalytic Testing

A modified testing procedure of the photocatalytic reactivity of the SGM was adapted from the International Organization for Standardization standard ISO 10678 [Fine ceramics (advanced ceramics, advanced technical ceramics); Determination of photocatalytic activity of surfaces in an aqueous medium by degradation of methylene blue] [48]. Methylene blue (MB^+) is a common contaminant in textile wastewater [49] and is routinely used as a surrogate to test organic pollutant reduction capacity. MB^+ degradation highlights the efficiency of photocatalytic degradation capabilities and is considered optimal for lab testing considerations because degradation of the structure results in a drastic color change from dark blue to clear as the progressive destruction of the compound forms CO_2 and H_2O byproducts [42,50]. Methylene blue possesses a high absorptivity with a maximum absorption occurring at a wavelength between 660 and 665 nm [51,52].

Photocatalytic testing of the SGM was performed using the batch reactor setup shown in Figure 1. 35 mL MB^+ solution was pipetted to cover a single layer of SGM adhered to the bottom of the batch reactor. SGM weighed approximately 3 grams per batch test, which equates to approximately 0.10 grams of photocatalyst depending upon the concentration of silicic acid under evaluation. UVA/B/C lights operating over a wide range of wavelengths from 550 to 250 nm were precisely placed above the targeted SGM at a height of 4". Experiments involving cycle testing required that the initial solution be discarded and another 35 mL of MB^+ pipetted onto the SGM which was then immediately placed back under the light. Minimal disturbances of the UV light source interacting with the targeted SGM were attempted and all deviations or movements of SGM, solution, and light interactions were kept at a minimum to insure replicability. Aliquots of solutions were extracted at various time intervals in order to obtain kinetic representation of the degradation potential. In addition, extracted aliquot solutions were cooled in a darkened container prior to further analysis. Concentrations of methylene blue analysis was conducted using a DR3900 Hach UV–Vis Spectrometer (UMKC) and identical matching 10ml quartz cuvettes. Prior to testing, calibration of the methylene blue was performed with MB^+ concentrations of 0, 10, 20, 30, 40, and 50 mg/L and a linear relationship of absorption to concentration was achieved. Full spectrum analysis indicated 660 nm was the primary peak wavelength for methylene blue examined in this study. Each aliquot sample analysis was performed in triplicate for absorbance at 660 nm, with full wavelength scans performed at least once per sample in order to determine when secondary or degradation peaks were observed.

Applications and Future Testing

An optimized SGM variation was finalized for a sustained photocatalytic reactivity and therefore treatment for organic contaminants in solution. The 50 mg/L SGM possessed the best treatment of MB^+ performance, however, variations to the design and treatment of pore space can be performed in order to target a specific waste stream. Amendments were added to the pore space with the intent to slowly diffuse through the thin shell and assist in treatment performance. Treatment within the pore space clearly show the diffusive abilities of the SGM while in contact with the waste stream. While these compounds did not necessarily have a positive impact on the degradation of MB^+, diffusion of various amendments from the pore space provides the additional capacity of the SGM to have either an electrophile or nucleophile attack on the contaminants of concern. Salts are known to decrease the surface tension in perfluoroalkyl acids [53] and can be used to improve removal efficiency of these compounds [54]. The utilization of the porous media introduces the ability to treat numerous contaminants and waste streams, with possibility to treat PFAS bearing waste streams.

Bench scale tests were performed for this study to determine the most feasible SGM as a packed bed or column water treatment system. While the performance of the SGM was established, additional work remains to be done. Future testing will be performed utilizing the media in a packed column (Figure 15). A column system will allow for continuous treatment of the waste stream in a very industrial driven design. SGM is optimal for this type of system as the gradation of the SGM can be controlled for, thus allowing treatment to be performed on the optimized gradation for contact time or reaction rates. Future testing on various organic contaminants, degradation kinetics, and flow rates in order to determine the required contact time and reaction rates.

Figure 31 – Rapid Testing Column Schematic.

Conclusion

A photocatalytic porous silica-based granular media was synthesized for continuous photocatalytic degradation of organic contaminants. Methylene blue was utilized as a surrogate contaminant for textile dyes. An initial testing matrix was utilized to determine a general method and process for synthesis of the SGM. The 3D structure of the polymer was retained through addition of a foaming agent, which has previously never been studied as a solvent extraction method. Further testing was performed on various ratios of silica to titania to determine a mixture design for a highly reactive and sustainable SGM. The porous structure allows for introduction of amendments that can be utilized in the degradation of the contaminants or as a pH buffer. The SGM was successful in removing over 90% of methylene blue in one hour and consistently performed at this for capacity in multiple successive cycles. The vast variability control of the SGM design allows for the media to be designed for general treatment purposes or tailored for a specific contaminant. Given the ease and low energy consumption of synthesis, the versatility of application, and continuous reactivity over time, the SGM is a promising media for treatment of organic contaminants in aqueous phase.

References

1. Lellis, B.; Fávaro-Polonio, C.Z.; Pamphile, J.A.; Polonio, J.C. Effects of textile dyes on health and the environment and bioremediation potential of living organisms. *Biotechnol. Res. Innov.* **2019**, *3*, 275–290, doi:10.1016/j.biori.2019.09.001.

2. Brillas, E.; Martínez-Huitle, C.A. Decontamination of wastewaters containing synthetic organic dyes by electrochemical methods. An updated review. *Appl. Catal. B Environ.* **2015**, *166–167*, 603–643, doi:10.1016/j.apcatb.2014.11.016.
3. Hassaan, M. A.; Nemr, A. El. Health and Environmental Impacts of Dyes: Mini Review. *Am. J. Environ. Sci. Eng.* **2017**, *1*, 64–67, doi:10.11648/j.ajese.20170103.11.
4. Raval, N.P.; Shah, P.U.; Shah, N.K. Malachite green "a cationic dye" and its removal from aqueous solution by adsorption. *Appl. Water Sci.* **2017**, *7*, 3407–3445, doi:10.1007/s13201-016-0512-2.
5. Khan, S.; Malik, A. Toxicity evaluation of textile effluents and role of native soil bacterium in biodegradation of a textile dye. *Environ. Sci. Pollut. Res.* **2018**, *25*, 4446–4458, doi:10.1007/s11356-017-0783-7.
6. Hueber-Becker, F.; Nohynek, G.J.; Dufour, E.K.; Meuling, W.J.; De Bie, A.T.; Toutain, H.; Bolt, H.M. Occupational exposure of hairdressers to [14C]-para-phenylenediamine-containing oxidative hair dyes: A mass balance study. *Food Chem. Toxicol.* **2007**, *45*, 160–169, doi:10.1016/j.fct.2006.08.002.
7. Cassano, A.; Molinari, R.; Romano, M.; Drioli, E. Treatment of aqueous effluents of the leather industry by membrane processes. *J. Membr. Sci.* **2001**, *181*, 111–126, doi:10.1016/s0376-7388(00)00399-9.
8. Albano, G.; Colli, T.; Nucci, L.; Charaf, R.; Biver, T.; Pucci, A.; Aronica, L.A. Synthesis of new bis[1-(thiophenyl)propynones] as potential organic dyes for colorless luminescent solar concentrators (LSCs). *Dyes Pigment.* **2020**, *174*, 108100, doi:10.1016/j.dyepig.2019.108100.

9. Samchetshabam, G.; Hussan, A.; Choudhury, T. G. Impact of Textile Dyes Waste on Aquatic Environments and its Treatment Impact of Textile Dyes Waste on Aquatic Environments and its Treatment. *Environ. Ecol.* **2017**, *35*, 2349—2353.
10. Chiu, Y.-H.; Chang, T.-F.M.; Chen, C.-Y.; Sone, M.; Hsu, Y.-J. Mechanistic Insights into Photodegradation of Organic Dyes Using Heterostructure Photocatalysts. *Catalysts* **2019**, *9*, 430, doi:10.3390/catal9050430.
11. Katafias, A.; Lipińska, M.; Strutyński, K. Alkaline hydrogen peroxide as a degradation agent of methylene blue—Kinetic and mechanistic studies. *React. Kinet. Mech. Catal.* **2010**, *101*, 251–266, doi:10.1007/s11144-010-0234-7.
12. Aa, O.; Aj, O. Kinetic Study of Decolorization of Methylene Blue with Sodium Sulphite in Aqueous Media: Influence of Transition Metal Ions. *J. Phys. Chem. Biophys.* **2014**, *2*, 1–7, doi:10.4172/2161-0398.1000136.
13. Ahmed, M.; Abou-Gamra, Z.; Salem, A. Photocatalytic degradation of methylene blue dye over novel spherical mesoporous Cr 2 O 3 /TiO 2 nanoparticles prepared by sol-gel using octadecylamine template. *J. Environ. Chem. Eng.* **2017**, *5*, 4251–4261, doi:10.1016/j.jece.2017.08.014.
14. Liu, H.; Guo, W.; Li, Y.; He, S.; He, C. Photocatalytic degradation of sixteen organic dyes by TiO2/WO3-coated magnetic nanoparticles under simulated visible light and solar light. *J. Environ. Chem. Eng.* **2018**, *6*, 59–67, doi:10.1016/j.jece.2017.11.063.
15. Zhu, S.; Wang, D. Photocatalysis: Basic Principles, Diverse Forms of Implementations and Emerging Scientific Opportunities. *Adv. Energy Mater.* **2017**, *7*, 1–24, doi:10.1002/aenm.201700841.

16. Akerdi, A.G.; Bahrami, S.H. Application of heterogeneous nano-semiconductors for photocatalytic advanced oxidation of organic compounds: A review. *J. Environ. Chem. Eng.* **2019**, *7*, 103283, doi:10.1016/j.jece.2019.103283.
17. Fujishima, A.; Honda, K. Electrochemical Photolysis of Water at a Semiconductor Electrode. *Nat. Cell Biol.* **1972**, *238*, 37–38, doi:10.1038/238037a0.
18. Fujishima, A.; Rao, T.N.; Tryk, D.A. Titanium dioxide photocatalysis. *J. Photochem. Photobiol. C Photochem. Rev.* **2000**, *1*, 1–21, doi:10.1016/s1389-5567(00)00002-2.
19. Martha, S.; Sahoo, P.C.; Parida, K.M. An overview on visible light responsive metal oxide based photocatalysts for hydrogen energy production. *RSC Adv.* **2015**, *5*, 61535–61553, doi:10.1039/c5ra11682a.
20. Belachew, N.; Kahsay, M.H.; Tadesse, A.; Basavaiah, K. Green synthesis of reduced graphene oxide grafted Ag/ZnO for photocatalytic abatement of methylene blue and antibacterial activities. *J. Environ. Chem. Eng.* **2020**, *8*, 104106, doi:10.1016/j.jece.2020.104106.
21. Hu, Z.; He, Q.; Ge, M. Photocatalytic degradation of organic contaminants by magnetic Ag3PO4/MFe2O4 (M = Zn, Ni, Co) composites: a comparative study and a new insight into mechanism. *J. Mater. Sci. Mater. Electron.* **2020**, *4*, doi:10.1007/s10854-020-04861-y.
22. Nuengmatcha, P.; Porrawatkul, P.; Chanthai, S.; Sricharoen, P.; Limchoowong, N.; Sricharoen, P. Enhanced photocatalytic degradation of methylene blue using Fe2O3/graphene/CuO nanocomposites under visible light. *J. Environ. Chem. Eng.* **2019**, *7*, 103438, doi:10.1016/j.jece.2019.103438.

23. Xu, B.; Ahmed, M.B.; Zhou, J.L.; Altaee, A.; Wu, M.; Xu, G. Photocatalytic removal of perfluoroalkyl substances from water and wastewater: Mechanism, kinetics and controlling factors. *Chemosphere* **2017**, *189*, 717–729, doi:10.1016/j.chemosphere.2017.09.110.

24. Dariani, R.; Esmaeili, A.; Mortezaali, A.; Dehghanpour, S. Photocatalytic reaction and degradation of methylene blue on TiO2 nano-sized particles. *Optik* **2016**, *127*, 7143–7154, doi:10.1016/j.ijleo.2016.04.026.

25. Liu, M.; Yin, W.; Qian, F.-J.; Zhao, T.-L.; Yao, Q.-Z.; Fu, S.-Q.; Zhou, G.-T. A novel synthesis of porous TiO2 nanotubes and sequential application to dye contaminant removal and Cr(VI) visible light catalytic reduction. *J. Environ. Chem. Eng.* **2020**, *8*, 104061, doi:10.1016/j.jece.2020.104061.

26. Xu, C.; Rangaiah, G.P.; Zhao, X.S. Photocatalytic Degradation of Methylene Blue by Titanium Dioxide: Experimental and Modeling Study. *Ind. Eng. Chem. Res.* **2014**, *53*, 14641–14649, doi:10.1021/ie502367x.

27. Grande, F.; Tucci, P. Titanium Dioxide Nanoparticles: A Risk for Human Health? *Mini Rev. Med. Chem.* **2016**, *16*, 762–769, doi:10.2174/1389557516666160321114341.

28. Poulopoulos, S.G.; Yerkinova, A.; Ulykbanova, G.; Inglezakis, V.J. Photocatalytic treatment of organic pollutants in a synthetic wastewater using UV light and combinations of TiO 2, H2 O2 and Fe (III). *PLoS ONE* **2019**, *14*, 1–20.

29. Khdary, N.H.; Alkhuraiji, W.S.; Sakthivel, T.S.; Khdary, D.N.; Salam, M.A.; Alshihri, S.; Al-Mayman, S.I.; Seal, S. Synthesis of Superior Visible-Light-Driven Nanophotocatalyst Using High Surface Area TiO_2 Nanoparticles Decorated with Cu_xO Particles. *Catalysts* **2020**, *10*, 872, doi:10.3390/catal10080872.

30. Luttrell, T.; Halpegamage, S.; Tao, J.; Kramer, A.; Sutter, E.A.; Batzill, M. Why is anatase a better photocatalyst than rutile?—Model studies on epitaxial TiO2 films. *Sci. Rep.* **2015**, *4*, 4043, doi:10.1038/srep04043.
31. Li, R.; Jia, Y.; Bu, N.; Wu, J.; Zhen, Q. Photocatalytic degradation of methyl blue using Fe 2 O 3 /TiO 2 composite ceramics. *J. Alloy. Compd.* **2015**, *643*, 88–93, doi:10.1016/j.jallcom.2015.03.266.
32. Lazar, M.A.; Varghese, S.; Nair, S.S. Photocatalytic Water Treatment by Titanium Dioxide: Recent Updates. *Catalysts* **2012**, *2*, 572–601, doi:10.3390/catal2040572.
33. Su, C.; Lin, K.-F.; Lin, Y.-H.; You, B.-H. Preparation and characterization of high-surface-area titanium dioxide by sol-gel process. *J. Porous Mater.* **2006**, *13*, 251–258, doi:10.1007/s10934-006-8012-7.
34. He, R.; Tsuzuki, T. Synthesis of high surface area amorphous tin-zinc oxides by a sol-gel method. In Proceedings of the 2010 International Conference on Nanoscience and Nanotechnology (ICONN 2010), Sydney, Australia, 22–26 February 2010; pp. 154–157, doi:10.1109/iconn.2010.6045224.
35. Nateq, M.H.; Ceccato, R. Sol-Gel Synthesis of TiO2 Nanocrystalline Particles with Enhanced Surface Area through the Reverse Micelle Approach. *Adv. Mater. Sci. Eng.* **2019**, *2019*, 1–14, doi:10.1155/2019/1567824.
36. Picco, S.; Villegas, L.; Tonelli, F.; Merlo, M.; Rigau, J.; Diaz, D.; Masuelli, M. Sol-Gel Processes of Functional Powders and Films. 2016. Available online: https://www.intechopen.com/books/chemical-reactions-in-inorganic-chemistry/sol-gel-processes-of-functional-powders-and-films (accessed on 12 February 2021).

37. Ola, O.O.; Maroto-Valer, M.M.; Liu, D.; Mackintosh, S.; Lee, C.-W.; Wu, J.C.S. Performance comparison of CO2 conversion in slurry and monolith photoreactors using Pd and Rh-TiO2 catalyst under ultraviolet irradiation. *Appl. Catal. B Environ.* **2012**, *126*, 172–179, doi:10.1016/j.apcatb.2012.07.024.
38. Yang, G.; Li, C. Electrofiltration of silica nanoparticle-containing wastewater using tubular ceramic membranes. *Sep. Purif. Technol.* **2007**, *58*, 159–165, doi:10.1016/j.seppur.2007.07.019.
39. Kuvayskaya, A.; Lotsi, B.; Mohseni, R.; Vasiliev, A. Mesoporous adsorbents for perfluorinated compounds. *Microporous Mesoporous Mater.* **2020**, *305*, 110374, doi:10.1016/j.micromeso.2020.110374.
40. Stebel, E.K.; Pike, K.A.; Nguyen, H.; Hartmann, H.A.; Klonowski, M.J.; Lawrence, M.G.; Collins, R.M.; Hefner, C.E.; Edmiston, P.L. Absorption of short-chain to long-chain perfluoroalkyl substances using swellable organically modified silica. *Environ. Sci. Water Res. Technol.* **2019**, *5*, 1854–1866, doi:10.1039/c9ew00364a.
41. Da Silva, R.C.; Kubaski, E.T.; Tenório-Neto, E.T.; Lima-Tenório, M.K.; Tebcherani, S.M. Foam glass using sodium hydroxide as foaming agent: Study on the reaction mechanism in soda-lime glass matrix. *J. Non Cryst. Solids* **2019**, *511*, 177–182, doi:10.1016/j.jnoncrysol.2019.02.003.
42. *ASTM C128-15. Standard Test Method for Relative Density (Specific Gravity) and Absorption of Fine Aggregate*; ASTM International: West Conshohocken, PA, 2015; Available online: www.astm.org (accessed on 12 February 2021).

43. Mills, A. An overview of the methylene blue ISO test for assessing the activities of photocatalytic films. *Appl. Catal. B Environ.* **2012**, *128*, 144–149, doi:10.1016/j.apcatb.2012.01.019.
44. Gurav, J.L.; Jung, I.-K.; Park, H.-H.; Kang, E.S.; Nadargi, D.Y. Silica Aerogel: Synthesis and Applications. *J. Nanomater.* **2010**, *2010*, 1–11, doi:10.1155/2010/409310.
45. Şahin, I.; Özbakır, Y.; Inönü, Z.; Ulker, Z.; Erkey, C. Kinetics of Supercritical Drying of Gels. *Gels* **2018**, *4*, 3, doi:10.3390/gels4010003.
46. Levy, D.; Zayat, M. *The Sol-Gel Handbook: Synthesis, Characterization, and Applications*, 1st ed.; Wiley-VCH Verlag GmbH & Co. KGaA: Weinheim, Germany, 2015.
47. Danks, A.; Hall, S.R.; Schnepp, Z. The evolution of 'sol–gel' chemistry as a technique for materials synthesis. *Mater. Horizons* **2016**, *3*, 91–112, doi:10.1039/c5mh00260e.
48. http://www.iso.org/iso/iso catalogue/catalogue tc/catalogue detail.htm? csnumber=46019 (accessed February, 2021)
49. Nibret, G.; Ahmad, S.; Rao, D.G.; Ahmad, I.; Shaikh, M.A.M.U.; Rehman, Z.U. Removal of Methylene Blue Dye from Textile Wastewater Using Water Hyacinth Activated Carbon as Adsorbent: Synthesis, Characterization and Kinetic Studies. *SSRN Electron. J.* **2019**, 1959–1969, doi:10.2139/ssrn.3358101.
50. Hou, C.; Hu, B.; Zhu, J. Photocatalytic Degradation of Methylene Blue over TiO2 Pretreated with Varying Concentrations of NaOH. *Catalysts* **2018**, *8*, 575, doi:10.3390/catal8120575.

51. Mills, A.; Hazafy, D.; Parkinson, J.; Tuttle, T.; Hutchings, M.G. Effect of alkali on methylene blue (C.I. Basic Blue 9) and other thiazine dyes. *Dyes Pigment.* **2011**, *88*, 149–155, doi:10.1016/j.dyepig.2010.05.015.

52. Milošević, M.D.; Logar, M.M.; Poharc-Logar, A.V.; Jakšić, N.L. Orientation and Optical Polarized Spectra (380–900 nm) of Methylene Blue Crystals on a Glass Surface. *Int. J. Spectrosc.* **2013**, *2013*, 1–6, doi:10.1155/2013/923739.

53. Pennell, K. (2020). Transport and Remediation of Per- and Polyfluoroalkyl Substances (PFAS) in the Subsurface.

54. Zhang, W.; Liang, Y. Removal of eight perfluoroalkyl acids from aqueous solutions by aeration and duckweed. *Sci. Total. Environ.* **2020**, *724*, 138357, doi:10.1016/j.scitotenv.2020.138357.

CHAPTER 4

CONCLUSIONS, FUTURE TESTING, AND RECOMMENDATIONS FOR IMPLEMENTATION

The research presented utilized laboratory batch reactor experiments to evaluate the ability of two photocatalytic materials to degrade methylene blue. One designed as an in-situ method for mitigating organic pollutants in stormwater, and the other an ex-situ method for degraded concentrated waste-streams. The study was intended to investigate the ability for the materials to degrade methylene blue over time, along with determining the sustainability of the photocatalytic properties. Concluding remarks, future testing, and recommendations for implementation will be addressed separately for the two materials tested in this study.

The first material testing was titanium dioxide immobilized within cement paste to be utilized in photocatalytic concrete infrastructures. While many photocatalytic cements are commercially available, many only are only capable of degrading air pollutants, and those able to degrade aqueous pollutants have a very short life cycle. Herein, the TiO_2 was functionalized to maleic anhydride to form (Ti-MAH) and inter-ground into the cement powder. Batch reactor testing of the Ti-MAH showed promising results with an increased reactivity when compared to TiO_2. Over 95% of methylene blue was completely degraded within 45 minutes and demonstrated a sustained reactivity within 5% over three cycles. Further testing shortened the cycles to 30 minutes; however, the shortened cycles revealed a secondary reaction mechanism, hydrolysis. The elevated pH originated from diffused calcium hydroxide in the hydrated cement and aided the degradation of the methylene blue, however, the degradation was still almost 12 times greater than that of the control without a photocatalyst. While these tests validated the photocatalytic reactivity of the Ti-MAH within cement paste, the theory that the

immobilized catalyst would be more sustainable than commercially available photocatalytic cements still needed to be tested. Four 30-minute cycles were tested with results showing the Ti-MAH cement was almost four times more efficient at degrading methylene blue by the fourth cycle when compared to a commercially available cement.

The current research was designed as a proof of concept to validate immobilizing the photocatalysts allows for a more efficient and sustainable photocatalytic cement. While this theory was proved out during the current study, more testing is needed before site implementation is possible. A scaled-up experiment is needed to determine the feasibility of Ti-MAH cement degrading organic contaminants in solution while flowing over the top of the cement. In addition, air pollution should be tested to determine if Ti-MAH cement can be translated to buildings instead of being limited to roadways, sidewalks, and gutters. Once future testing is complete, a better understanding of where Ti-MAH cement can be placed will occur.

The second material tested was a silica-based granular media (SGM) designed for ex-situ remediation of organic contaminants in solution. The current study goes in depth into the material characteristics and mixture proportion optimization of the media designed to translate from batch reactors to column reactors. A general process was developed which introduced the titanium dioxide into the sol-gel matrix. After gelation occurred a foaming agent was added and the media was fired to create what is denoted at SGM. The study utilized various concentrations of silicic acid which were tested to determine the optimum proportions for efficient photocatalytic reactivity. Along with silica concentration, the impacts of pH were also tested, and degradation kinetics were determined.

The current study was designed to be initial batch reactor testing for future research which will involve column testing of various organic contaminant solution. Both small- and large-scale column reactors have been designed and fabricated. Future testing will include concentrated waste-streams containing per- and polyfluoroalkyl substances (PFAS), 1,4-dioxane, and personal care products. Through a series of testing matrixes, the SGM will be evaluated for its ability to degrade these contaminants will the intension of scaling up to a pilot-test.

VITA

Hannah Marie McIntyre was born on April 6, 1998 in Kansas City, MO. She attended high school at Raytown South Senior High. After graduation high school, she started college at the University of Missouri – Kansas City where she received her bachelor's in civil engineering. As an undergraduate, Hannah served as the vice president/project manager of UMKC's chapter of engineers without borders and traveled to El Vallecito, Panama to do surveying and maintenance on a water distribution system previously installed by the same group. Hannah started research at UMKC during her senior year and was awarded the UMKC SEARCH grant. She has presented her research at three conferences and has been invited to speak at a webinar in collaboration with an industrial partner on her novel destructive technology for PFAS. She has also published some of her master's research in *Catalyst.* As a master's student, Hannah was awarded the UMKC Graduate Assistant (GAF) fellowship and the ACI Dr. David Richardson scholarship. Upon her graduation, she plans to continue to pursue her Ph.D. at UMKC.